# Hadron Polarizabilities

Barry R. Holstein
Department of Physics-LGRT
University of Massachusetts
Amherst, MA 01003 USA
and
Stefan Scherer
PRISMA Center of Excellence
Institut für Kernphysik
Johannes Gutenberg-Universität Mainz
D-55099 Mainz, Germany

December 31, 2013

**Abstract**

Electromagnetic polarizabilities describe the response of a system to the application of an external quasi-static electric or magnetic field. In this article experimental and theoretical work addressing the polarizabilities of the light hadrons is examined.

1

# 1 Introduction

The concept of polarizability is well known from classical electrodynamics, where the electric and magnetic polarizabilities $\alpha_E, \beta_M$ are simply the coefficients of proportionality between applied quasi-static electric/magnetizing fields and the resultant *induced* electric/magnetic dipole moments [1]. As discussed below, this concept is also applicable to hadronic systems, where the applied fields are provided by electromagnetic radiation and the measurements are performed via Compton scattering [2, 3, 4, 5, 6, 7, 8, 9, 10]. In this regard, polarizabilities provide the leading-order correction to the well-known Thomson scattering amplitude and a series of experiments have measured $\alpha_E, \beta_M$ for various hadronic systems such as the proton [11, 12, 13, 14, 15], the neutron [16, 17, 18, 19], and even the charged pion [20, 21, 22, 23, 24, 25]. Such quantities provide valuable information concerning hadronic structure and are fundamental properties [4, 5] which are now included by the particle data group in their listings [26]. At the same time, they are also discussed in the context of precision determinations of other physical observables such as the Lamb shift in muonic hydrogen [27, 28] and the hadronic light-by-light contribution to the muon anomalous magnetic moment [29]. At higher order there exist additional *spin-dependent* and *spin-independent* polarizabilities which provide new structure probes and are just now beginning to be measured experimentally [30, 31, 32, 33]. Information about the distribution of polarizability structure within the proton has been provided by virtual Compton scattering measurements [34, 35, 36, 37, 38, 39]. On the theoretical side there exists a great deal of work in the literature involving the analysis of Compton scattering, both real and virtual, in terms of polarizabilities, using hadronic models as well as with more rigorous methods such as the use of dispersion theory [40, 41] and/or effective field theory (chiral perturbation theory) [42, 43].

The purpose of this article is to provide an overview of the existing body of theoretical and experimental probes of electromagnetic polarizabilities as well as to provide a blueprint for possible future work. In Sec. 2, we introduce the basic concept of electric and magnetic (scalar, *i.e.*, spin-independent) polarizabilities and examine their experimental determination as well as various theoretical approaches to these quantities. In Sec. 3, we examine the corresponding spin-dependent (vector) polarizabilities which arise at one higher order in the Compton amplitude, discussing the theoretical predictions for such quantities as well as ongoing experimental programs which seek to mea-

sure them. In Sec. 4, we look at even higher-order polarizabilities and compare theoretical predictions to results obtained from dispersive approaches to Compton scattering. In Sec. 5, we discuss how virtual Compton scattering has been used in order to determine polarizability distributions within the proton. Finally, in a concluding Section 6, we present a brief summary of what has been learned as well as a glimpse into possible future work in this area.

# 2 Scalar Polarizabilities

## 2.1 Macroscopic Systems

In classical physics when elementary systems having structure are probed via application of an external electric field, various responses are conceivable. In the simplest case, the applied field leads to a charge separation and thereby to an induced electric dipole moment, with positive (negative) charges moving in the direction (opposite to the direction) of the field [1]. In the case of orientation polarization, preexisting but initially randomly oriented permanent dipole moments are lined up by the applied field. In anisotropic materials, even though the polarization still depends linearly on the field, its direction is not necessarily parallel to the applied field but is determined in terms of a polarizability tensor of second rank [44]. Finally, in ferroelectric materials the polarization is a nonlinear function of the electric field showing, in addition, a hysteresis effect.

In the first of the above cases, the electric polarizability $\alpha_E$ of a system is simply the constant of proportionality between the applied static and uniform field $\mathbf{E}$ and the induced electric dipole moment $\mathbf{p}$,

$$\mathbf{p} = 4\pi\alpha_E\mathbf{E}, \tag{1}$$

corresponding to a potential energy

$$U_E = -\frac{1}{2}4\pi\alpha_E\mathbf{E}^2, \quad i.e., \quad \mathbf{p} = -\frac{\partial U_E}{\partial \mathbf{E}}. \tag{2}$$

The factor of $4\pi$ is related with the (standard) use of Gaussian units for the polarizabilities but natural units in field-theoretical calculations. Clearly the electric polarizability is expected to be a positive quantity and its magnitude

2

provides a measure of the "stiffness" or resistance to deformation of the system.

Similarly, when a static and uniform magnetizing field $\mathbf{H}$ is applied to such an elementary system there are two competing mechanisms at work. On the one hand, if the fundamental constituents of the system themselves possess intrinsic magnetic dipole moments, they tend to align in the direction of the applied field, producing a positive (paramagnetic) effect. On the other hand, by Lenz' law an applied field induces currents which produce an induced magnetic moment opposite to this field, yielding a negative (diamagnetic) effect. Using the definition

$$\mathbf{m} = 4\pi\beta_M\mathbf{H}, \tag{3}$$

corresponding to a potential energy

$$U_H = -\frac{1}{2}4\pi\beta_M\mathbf{H}^2, \quad i.e., \quad \mathbf{m} = -\frac{\partial U_H}{\partial \mathbf{H}}, \tag{4}$$

the magnetic polarizability can be either positive of negative depending on which mechanism is dominant.

An equivalent means of expressing these results is in terms of the energy density of a dilute macroscopic collection of such polarizable particles randomly distributed within a volume $V$. If $N(\mathbf{x})$ is the number density of these particles then the energy density of the (dilute) system including polarizability effects is given by

$$u(\mathbf{x}) = \frac{1}{2}\mathbf{E}_0^2(\mathbf{x})(1 - 4\pi N(\mathbf{x})\alpha_E) + \frac{1}{2}\mathbf{H}_0^2(\mathbf{x})(1 - 4\pi N(\mathbf{x})\beta_M), \tag{5}$$

where $\mathbf{E}_0$ and $\mathbf{H}_0$ denote given external electric and magnetic fields applied to the medium. For the moment we assume a constant and uniform number density $N$. Comparing with the definition of the dielectric constant $\epsilon$ and magnetic susceptibility $\mu$,

$$u = \frac{1}{2}\epsilon\mathbf{E}^2 + \frac{1}{2}\mu\mathbf{H}^2, \tag{6}$$

where

$$\mathbf{E} = (1 - 4\pi N\alpha_E)\mathbf{E}_0 \quad \text{and} \quad \mathbf{H} = (1 - 4\pi N\beta_M)\mathbf{H}_0 \tag{7}$$

are the net fields in the presence of the induced dipoles, we see that at the classical level we identify at leading order in the number density

$$\epsilon = 1 + 4\pi N\alpha_E \quad \text{and} \quad \mu = 1 + 4\pi N\beta_M. \tag{8}$$

Thus Eq. (8) provides a way to determine the polarizabilities via measurement of $\epsilon, \mu$ or of the index of refraction, which is given by

$$n = \sqrt{\epsilon\mu} \simeq 1 + 2\pi N(\alpha_E + \beta_M). \tag{9}$$

Since $N\alpha_E, N\beta_M$ must be dimensionless, we see that the electric and magnetic polarizabilities $\alpha_E$, $\beta_M$ have units of volume.

A simple example of this phenomenon is provided by the hydrogen atom. In a classical picture, if we represent the atom as an electron bound to a proton via a harmonic oscillator potential with frequency $\omega_0$, application of an electric field $\mathbf{E}$ generates a charge separation

$$\boldsymbol{\delta} = \mathbf{r}_e - \mathbf{r}_p = -\frac{e\,\mathbf{E}}{m_r\omega_0^2}, \tag{10}$$

where $e$ is the proton charge and $m_r = m_p m_e/(m_p + m_e)$ is the reduced mass. The resultant electric dipole moment is

$$\mathbf{p} = -e\,\boldsymbol{\delta} = \frac{e^2\mathbf{E}}{m_r\omega_0^2} \tag{11}$$

which, using

$$U_E = -\frac{1}{2}\mathbf{p} \cdot \mathbf{E} \tag{12}$$

for the potential energy of an induced dipole moment in an external field, corresponds to an electric polarizability

$$\alpha_E = \frac{\alpha_{\mathrm{em}}}{m_r\omega_0^2}, \tag{13}$$

where $\alpha_{\mathrm{em}} = e^2/4\pi \approx 1/137$ is the fine-structure constant. Utilizing a value for $\omega_0$ corresponding to the rotational frequency of the hydrogen ground state—$\omega_0 = \alpha_{\mathrm{em}}^2 m_r/2$—we have then

$$\alpha_E^H = \frac{4}{\alpha_{\mathrm{em}}^3 m_r^3} = \frac{3}{\pi}V_H, \tag{14}$$

where $V_H = 4\pi a_0^3/3$, with $a_0 = 1/(m_r\alpha_{\mathrm{em}})$ being the Bohr radius, is the volume of the hydrogen atom. In a fully quantum mechanical calculation, the hydrogen atom polarizability can be exactly calculated. Using the interaction potential

$$V_{\mathrm{int}} = -(-e\,\mathbf{r}) \cdot \mathbf{E} = e\,\mathbf{r} \cdot \mathbf{E}, \tag{15}$$

4

we have in second-order perturbation theory

$$\Delta E_0^{(2)} = -e^2 \sum_{n \neq 0} \frac{\langle 0 | \mathbf{r} \cdot \mathbf{E} | n \rangle \langle n | \mathbf{r} \cdot \mathbf{E} | 0 \rangle}{E_n - E_0}. \tag{16}$$

Equating $\Delta E_0^{(2)} = U_E = -2\pi \alpha_E^H \mathbf{E}^2$, choosing $\mathbf{E}$ along the $z$-axis, and performing the intermediate state summation, we find [45]

$$\alpha_E^H = 2\alpha_{\rm em} \sum_{n \neq 0} \frac{\langle 0 | z | n \rangle \langle n | z | 0 \rangle}{E_n - E_0} = \frac{9}{2a_0^3} = \frac{27}{8\pi} V_H, \tag{17}$$

so that again we determine that $\alpha_E^H \sim V_H$.

The magnetic polarizability of the hydrogen atom is much smaller than its electric counterpart. Classically $\beta_M^H$ can be estimated via turning on a uniform magnetizing field $\mathbf{H} = H(t)\,\hat{\mathbf{e}}_z$ in the vicinity of the atom. If the center of the atom is at the origin and one considers a closed circle of radius $\rho$ in the $(x, y)$ plane concentric with the origin, the changing magnetic field leads via Faraday's law to a circulating electric field $\mathbf{E} = E(\rho, t)\,\hat{\mathbf{e}}_\phi$ [46],

$$2\pi\rho E(\rho, t) = -\frac{d}{dt}\left[\pi\rho^2 H(t)\right] \quad \text{yielding} \quad E = -\frac{\rho}{2}\frac{dH}{dt}. \tag{18}$$

The resulting torque on an electron generates an angular momentum change

$$\frac{d\mathbf{L}}{dt} = \rho\,\hat{\mathbf{e}}_\rho \times (-eE\,\hat{\mathbf{e}}_\phi) = e\frac{\rho^2}{2}\frac{dH}{dt}\,\hat{\mathbf{e}}_z. \tag{19}$$

Integrating with respect to time from zero field, results in an extra angular momentum

$$\Delta\mathbf{L} = e\frac{\rho^2}{2}H\,\hat{\mathbf{e}}_z, \tag{20}$$

producing an additional orbital magnetic moment

$$\Delta\boldsymbol{\mu} = -\frac{e}{2m_r}\Delta\mathbf{L} = -\frac{e^2\langle r^2 \rangle}{6m_r}H\,\hat{\mathbf{e}}_z, \tag{21}$$

where we have used spherical symmetry to write $\langle x^2 + y^2 \rangle = \frac{2}{3}\langle r^2 \rangle$. According to Lenz' law, the added moment is indeed opposite to the magnetic field. Using $U_M = -\Delta\boldsymbol{\mu} \cdot \mathbf{H}/2$, we find then a negative magnetic polarizability

$$\beta_M^H = -\frac{\alpha_{\rm em}a_0^2}{6m_r} = -\frac{1}{6\alpha_{\rm em}m_r^3} = -\frac{1}{24}\alpha_{\rm em}^2\alpha_E^H \sim 10^{-6}V_H, \tag{22}$$
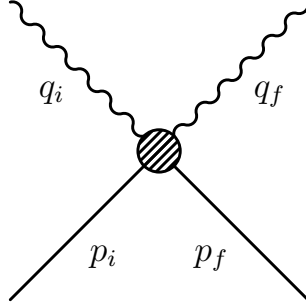
5

Figure 1: Compton scattering kinematics

with $\alpha_E^H$ of Eq. (14). The analogous result can be obtained quantum mechanically by considering a static and uniform external magnetizing field in the positive $z$ direction, $\mathbf{H} = H\hat{\mathbf{e}}_z$, giving rise to a perturbation

$$V_{\text{int}} = \frac{e}{2m_r}l_z H + \frac{e^2}{8m_r}(x^2 + y^2)H^2 = H_1 + H_2, \qquad (23)$$

where $l_z$ is the $z$ component of the relative orbital angular momentum operator. Applying second-order perturbation theory results in

$$\Delta E_0^{(2)} = \langle 0|H_2|0\rangle - \sum_{n \neq 0} \frac{|\langle n|H_1|0\rangle|^2}{E_n - E_0} = \frac{2}{3}\langle r^2\rangle \frac{e^2 H^2}{8m_r}, \qquad (24)$$

since $l_z|0\rangle = 0$. Equating $\Delta E_0^{(2)} = U_M = -2\pi\beta_M^H \mathbf{H}^2$ and comparing with Eq. (22), we find exactly the same result for $\beta_M^H$ as found in the classical physics derivation.

## 2.2   Hadron Polarizabilities

Next we move to consider the polarizabilities of strongly interacting particles, namely, hadrons. We begin with a simple charged spinless particle such as, e.g., a $\pi^+$. Because the particle is charged, the use of macroscopic samples and a constant external electric field is not feasible. Instead one uses the fields generated in a Compton scattering process, $\gamma(q_i) + \pi^+(p_i) \rightarrow \gamma(q_f) + \pi^+(p_f)$ (see Fig. 1). In this case when the wavelength of the photon is much larger than that of the target, any structure of the particle cannot be resolved and

6

Table 1: Thomson cross section $\sigma_T$ for the electron, charged pion, and proton

| Particle | $\sigma_T$ |
|----------|------------|
| Electron | 0.665 barn |
| Pion | 8.84 $\mu$barn |
| Proton | 197 nbarn |

it is characterized only by its charge $e$ and mass $M$. The Hamiltonian is then the simple Schrödinger form relevant for a charged particle in the presence of an external electromagnetic four-vector potential $A^\mu = (\phi, \mathbf{A})$ [1]

$$H_0 = \frac{(\mathbf{p} - e\mathbf{A})^2}{2M} + e\phi. \tag{25}$$

Using the Lorenz condition $\partial_\mu A^\mu = 0$ and the Coulomb gauge $\phi = A^0 = 0$, the corresponding transition amplitude has the Thomson form

$$T_0^{\text{Compton}} = -\frac{e^2}{M}\, \hat{\boldsymbol{\epsilon}}_f^* \cdot \hat{\boldsymbol{\epsilon}}_i, \tag{26}$$

leading to the well-known (laboratory frame) Thomson cross section [46, 47]

$$\frac{d\sigma_{\text{Compton}}}{d\Omega} = \frac{\alpha_{\text{em}}^2}{2M^2}\frac{\omega_f^2}{\omega_i^2}(1 + \cos^2\theta). \tag{27}$$

The total Thomson cross section, obtained by taking the limit $\omega_i \to 0$ and integrating over the entire solid angle, reproduces the classical Thomson scattering cross section denoted by $\sigma_T$,

$$\sigma_T = \frac{8\pi}{3}\frac{\alpha_{\text{em}}^2}{M^2}. \tag{28}$$

Numerical values of $\sigma_T$ for the electron, charged pion, and the proton are shown in Table 1.

As the wavelength becomes smaller and comparable to the size of the target, the particle begins to be resolved and the simple Schrödinger Hamiltonian $H_0$ is augmented by a form which includes polarizability corrections [2],

$$H = H_0 - \frac{1}{2}4\pi\alpha_E\mathbf{E}^2 - \frac{1}{2}4\pi\beta_M\mathbf{H}^2 + \dots. \tag{29}$$

The Compton amplitude becomes then

$$T_{\text{Compton}} = \hat{\boldsymbol{\epsilon}}_f^* \cdot \hat{\boldsymbol{\epsilon}}_i \left( -\frac{e^2}{M} + 4\pi\alpha_E\omega_f\omega_i \right) + 4\pi\beta_M\hat{\boldsymbol{\epsilon}}_f^* \times \mathbf{q}_f \cdot \hat{\boldsymbol{\epsilon}}_i \times \mathbf{q}_i + \ldots, \quad (30)$$

while the cross section is

$$\frac{d\sigma_{\text{Compton}}}{d\Omega} = \frac{1}{M^2}\frac{\omega_f^2}{\omega_i^2} \left\{ \frac{\alpha_{\text{em}}^2}{2}(1 + \cos^2\theta) - \alpha_{\text{em}}M\omega_f\omega_i \left[ \frac{1}{2}(\alpha_E + \beta_M)(1 + \cos\theta)^2 \right.\right.$$
$$\left.\left. +\frac{1}{2}(\alpha_E - \beta_M)(1 - \cos\theta)^2 \right] + \ldots \right\}, \quad (31)$$

so that $\alpha_E, \beta_M$ can be determined by a careful measurement of the angular distribution in Compton scattering.

## 2.3   Proton Polarizabilities

In the case of the proton, there exists an additional contribution due to the feature that the proton possesses a magnetic moment (mm). Thus a piece

$$H_{\text{mm}} = -\boldsymbol{\mu}_p \cdot \mathbf{H} \quad (32)$$

must be appended to the interaction Hamiltonian. The magnetic moment is given by

$$\boldsymbol{\mu}_p = g_p\,\mu_N\mathbf{S}, \quad (33)$$

where $g_p = 5.59$ is the proton gyromagnetic ratio, $\mu_N = e/(2m_p)$ the nuclear magneton, and $\mathbf{S}$ the spin operator. The corresponding relativistic cross section in the absence of the polarizability terms is the Powell cross section [48] and an experimental search for polarizabilities seeks deviations from this form. An important consideration here is the photon energy. The size of such polarizability terms compared to the leading Thomson amplitude is

$$\sim 2\alpha_E^p \frac{m_p\omega^2}{\alpha_{\text{em}}} \approx 33\frac{\omega^2}{m_p^2}, \quad (34)$$

where we made use of the empirical value $\alpha_E^p = 11.2 \times 10^{-4}\,\text{fm}^3$. In order to produce a sizable polarizability effect without bringing in large contributions from higher-order terms the photon energy is ideally in the 50–100 MeV range. However, in this case and even more so for the case of larger energies

it is necessary to have an estimate for the contribution of higher-order effects and this is generally provided by various dispersion relation codes (see, e.g., Refs. [40, 41]) or effective-field-theory calculations (see, e.g., Refs. [49, 50, 51]). In this fashion a series of measurements on the proton [11, 12, 13, 14, 15] has yielded the rather precise numbers [26]:

$$\alpha_E^p = (11.2 \pm 0.4) \times 10^{-4} \, \text{fm}^3 \quad \text{and} \quad \beta_M^p = (2.5 \mp 0.4) \times 10^{-4} \, \text{fm}^3. \quad (35)$$

In terms of the proton volume—$V_p = \frac{4\pi}{3} \langle (r_E^p)^2 \rangle^{\frac{3}{2}}$—we have then $\alpha_E^p \sim 4 \times 10^{-4} \, V_p$, showing that the proton is much stiffer and more strongly bound than the hydrogen atom.

Another interesting feature of these experimental results comes from the magnetic polarizability. The $\Delta$ pole diagram makes a rather strong paramagnetic contribution [52]

$$\beta_M^p(\Delta - \text{pole}) \sim 10 \times 10^{-4} \, \text{fm}^3 \quad (36)$$

so that the fact that the experimental number is only about 25 % of this value reveals a very strong diamagnetic contribution, presumably from the meson cloud. Such a picture is qualitatively supported by the Skyrme model [53].

## 2.4  Dispersion Relations

An alternative approach to the size of the polarizabilities comes from the use of causality via dispersion relations [54]. In the case of forward Compton scattering, we can write

$$T_{\text{forward}} = 4\pi f_0(\omega) \hat{\boldsymbol{\epsilon}}_f^* \cdot \hat{\boldsymbol{\epsilon}}_i + 4\pi i g_0(\omega) \boldsymbol{\sigma} \cdot \hat{\boldsymbol{\epsilon}}_f^* \times \hat{\boldsymbol{\epsilon}}_i, \quad (37)$$

where the subscripts 0 refer to $\theta = 0°$. Equation (37) needs to be evaluated between Pauli spinors of the initial and final nucleons, respectively. In the case of the spin-averaged (scalar) amplitude $f_0(\omega)$, the imaginary part is given by the optical theorem via

$$\text{Im} \, [f_0(\omega)] = \frac{\omega}{4\pi} \sigma_{\text{tot}}(\omega), \quad (38)$$

where $\sigma_{\text{tot}}(\omega)$ is the total photoabsorption cross section. Using $f_0^*(\omega) = f_0(-\omega)$ and applying Titchmarsh's theorem [55] to $(f_0(\omega) - f_0(0))/\omega^2$, the

corresponding real part of the proton scattering amplitude can be written as

$$\text{Re}\left[f_0^p(\omega)\right] = -\frac{\alpha_{\text{em}}}{m_p} + \frac{\omega^2}{2\pi^2}P\int_0^\infty d\omega' \frac{\sigma_{\text{tot}}^p(\omega')}{\omega'^2 - \omega^2}, \tag{39}$$

where we have performed a subtraction since the presence of the Thomson amplitude indicates that an unsubtracted dispersion relation does not converge. Expanding the scattering amplitude below the pion production threshold via

$$f_0^p(\omega) = -\frac{\alpha_{\text{em}}}{m_p} + \left(\alpha_E^p + \beta_M^p\right)\omega^2 + \dots \tag{40}$$

leads to the Baldin sum rule [56]

$$\alpha_E^p + \beta_M^p = \frac{1}{2\pi^2}\int_0^\infty d\omega \frac{\sigma_{\text{tot}}^p(\omega)}{\omega^2} \tag{41}$$

which relates the sum of electric and magnetic polarizabilities to a weighted integral over the total photoabsorption cross section. In the case of the proton, using experimental cross section numbers, rather precise values have been calculated:

$$\alpha_E^p + \beta_M^p = \begin{cases} (13.69 \pm 0.14) \times 10^{-4}\,\text{fm}^3 \text{ [57]}, \\ (14.0 \pm 0.5) \times 10^{-4}\,\text{fm}^3 \text{ [58]}, \\ (13.8 \pm 0.4) \times 10^{-4}\,\text{fm}^3 \text{ [15]}. \end{cases} \tag{42}$$

In order to separate the electric and magnetic polarizabilities, one can use a backward dispersion relation, the Bernabeu-Ericson-Ferro Fontan-Tarrach (BEFT) sum rule, to determine $\alpha_E - \beta_M$, which takes the form [59, 60]

$$(\alpha_E^p - \beta_M^p)^{\text{BEFT}} = (\alpha_E^p - \beta_M^p)_s + (\alpha_E^p - \beta_M^p)_t. \tag{43}$$

Here, the $s$-channel contribution is given by

$$(\alpha_E^p - \beta_M^p)_s = \frac{1}{2\pi^2}\int_0^\infty \frac{d\omega}{\omega^2}\left(1 + \frac{2\omega}{m_p}\right)^{\frac{1}{2}}\left(\sigma^p(\omega, \text{yes}) - \sigma^p(\omega, \text{no})\right), \tag{44}$$

where $\sigma(\omega, \Delta P)$ represents components of the photoabsorption cross section associated with multipoles which change ($\Delta P = \text{yes}$), do not change ($\Delta P = \text{no}$) parity. Numerical evaluation of Eq. (44) is reasonably robust and yields [61]

$$(\alpha_E^p - \beta_M^p)_s = -5.0 \times 10^{-4}\,\text{fm}^3. \tag{45}$$

10

Calculation of the $t$-channel contribution requires summation over a complete set of intermediate-state contributions to $p\bar{p} \to$ hadrons $\to \gamma\gamma$. The lightest such state is $\pi\pi$ and is dominated by low-partial-wave contributions. Including only $S$- and $D$-wave pieces, we have [62]

$$(\alpha_E^p - \beta_M^p)_t = \frac{1}{16\pi^2} \int_{4M_\pi^2}^{\infty} \frac{dt}{t^2} \frac{16}{4m_p^2 - t} \sqrt{\frac{t - 4M_\pi^2}{t}}$$
$$\times \left[ f_+^{p\,0}(t) F_0^{0*}(t) - \left( m_p^2 - \frac{t}{4} \right) \left( \frac{t}{4} - M_\pi^2 \right) f_+^{p\,2}(t) F_0^{2*}(t) + \dots \right],$$
$$(46)$$

where $f_+^{p\,J}(t)$ are partial-wave amplitudes for $p\bar{p} \to \pi\pi$ and $F_0^{J*}(t)$ are the corresponding amplitudes for $\pi\pi \to \gamma\gamma$. Past evaluations have yielded a range of values for this contribution, namely, from $10.3 \times 10^{-4}\,\mathrm{fm}^3$ to $16.1 \times 10^{-4}\,\mathrm{fm}^3$ for the $S$-wave piece and $-1.3 \times 10^{-4}\,\mathrm{fm}^3$ for the $D$ wave [62]. In the case that the $S$ wave dominates, one approach is to use the $\sigma$-pole contribution to estimate this value—

$$(\alpha_E^p - \beta_M^p)_t \simeq \frac{g_{\sigma NN} \mathcal{M}(\sigma \to \gamma\gamma)}{2\pi M_\sigma^2}. \tag{47}$$

Using a simple Nambu-Jona-Lasinio model, we find for the $\sigma NN$ coupling constant $g_{\sigma NN} = g_{\pi NN} = 13.12$ [63] and [64]

$$M_\sigma = \left( \frac{16\pi^2}{N_c} F_\pi^2 + M_\pi^2 \right)^{\frac{1}{2}}, \tag{48}$$

where $F_\pi = 92.2$ MeV [26] is the pion-decay constant and $N_c = 3$ the number of colors. Thus

$$\mathcal{M}(\sigma \to \gamma\gamma) = \frac{3\alpha_{\mathrm{em}}}{\pi F_\pi} \left[ \left( \frac{2}{3} \right)^2 + \left( -\frac{1}{3} \right)^2 \right] \tag{49}$$

and

$$(\alpha_E^p - \beta_M^p)_t = 15.2 \times 10^{-4}\,\mathrm{fm}^3. \tag{50}$$

In combination with $(\alpha_E^p + \beta_M^p) = 14.0 \times 10^{-4}\,\mathrm{fm}^3$ [58], this result yields

$$\alpha_E^p = 12.1 \times 10^{-4}\,\mathrm{fm}^3 \quad \text{and} \quad \beta_M^p = 1.9 \times 10^{-4}\,\mathrm{fm}^3 \tag{51}$$

in good agreement with direct measurements. However, a definitive numerical approach to the $t$-channel contribution remains to be achieved.

## 2.5 Theoretical Approaches

That the size of the nucleon polarizabilities are reasonable can be seen from a simple nonrelativistic harmonic oscillator valence quark model calculation [65]. Denoting the proton ground state by $|0\rangle_p$, we can use the result [66, 67, 68]

$$\alpha_E^p = \frac{\alpha_{\text{em}}}{3m_p}\,_p\langle 0|r_E^2|0\rangle_p + 2\alpha_{\text{em}} \sum_{n\neq 0} \frac{|\langle n|D_z|0\rangle_p|^2}{E_n - E_0} \qquad (52)$$

with the mean-square charge radius and electric dipole operators, respectively,

$$r_E^2 = \sum_{i=1}^{3} q_i(\mathbf{r}_i - \mathbf{R})^2, \quad \mathbf{D} = \sum_{i=1}^{3} q_i(\mathbf{r}_i - \mathbf{R}),$$

where $\mathbf{R}$ is the center-of-mass coordinate. Here the oscillator frequency $\omega_0$ can be found in terms of the charge radius via

$$\omega_0 = \frac{3}{m_p\langle (r_E^p)^2\rangle} \simeq 160\,\text{MeV} \qquad (53)$$

and the predicted electric polarizability becomes [5]

$$\alpha_E^p = \frac{2\alpha_{\text{em}}m_p}{9}\langle (r_E^p)^2\rangle^2 \simeq 46 \times 10^{-4}\,\text{fm}^3 \qquad (54)$$

which is in the ballpark but is about a factor of four too large. This overprediction can be understood in terms of the feature that the predicted oscillator frequency, which measures the excitation energy, is somewhat too small. If a more reasonable value of $\sim 300$ MeV is used, the number comes out about right. In any case we see that the size of the electric polarizability—$\alpha_E \sim 10^{-3}\,V$—is not unreasonable.

The treatment of the magnetic polarizability is more challenging, but in any case a constituent quark model is not expected to be successful, as long as it does not deal with the pion cloud, which should be an important component of any realistic nucleon model. In this regard the use of chiral perturbation theory (ChPT) [69, 42, 43] is promising (see, e.g., Refs. [70, 71, 72, 73] for an introduction). In ChPT physical observables are calculated perturbatively in terms of a momentum expansion in $q/\Lambda_\chi$. The chiral-symmetry-breaking scale $\Lambda_\chi$ is $4\pi F_\pi \sim 1$ GeV [74, 75] and $q$ collectively
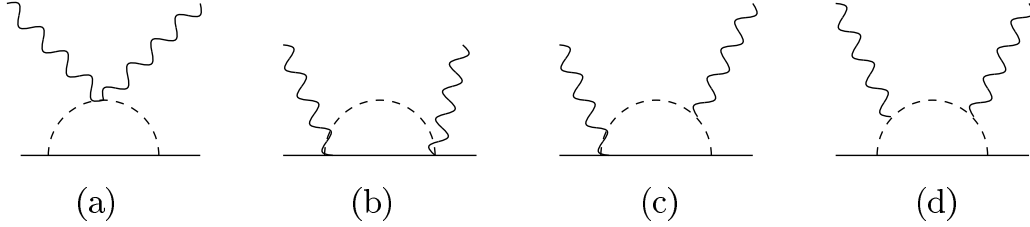
Figure 2: One-loop diagrams in HBChPT. Crossed diagrams are not shown.

stands for a quantity small in comparison to $\Lambda_\chi$ such as the pion mass, small external four-momenta of the pion, and small external three-momenta of the nucleon. The first such calculation of the proton polarizability was that of Bernard, Kaiser, and Meißner, which was performed using relativistic ChPT [43] at the one-loop level. The results were obtained in a closed (Feynman parameter) integral form and their chiral expansion in terms of $\mu = M_\pi/m_N$ reads [76]

$$
\begin{aligned}
\alpha_E^p &= \frac{\alpha_{\text{em}} g_A^2}{48\pi^2 F_\pi^2 m_N} \left[ \frac{5\pi}{2\mu} + 18\ln\mu + \frac{33}{2} + \mathcal{O}(\mu) \right] = 7.9 \times 10^{-4}\,\text{fm}^3, \\
\beta_M^p &= \frac{\alpha_{\text{em}} g_A^2}{48\pi^2 F_\pi^2 m_N} \left[ \frac{\pi}{4\mu} + 18\ln\mu + \frac{63}{2} + \mathcal{O}(\mu) \right] = -2.3 \times 10^{-3}\,\text{fm}^3,
\end{aligned}
\tag{55}
$$

where the numerical values refer to the full expressions. Note that the expressions of Eq. (55) for the polarizabilities contain no free parameters, *i.e.*, they are entirely expressed in terms of $M_\pi$, $m_N$, $F_\pi$, and the axial-vector coupling constant $g_A = 1.27$. However, manifestly Lorentz-invariant (or relativistic) ChPT (RChPT) seemingly had a problem concerning power counting when loops containing internal nucleon lines come into play. In some cases, a diagram apparently has contributions which are of lower order than determined by the power counting [43]. Therefore, the calculation was redone using the methods of heavy-baryon ChPT (HBChPT) [77, 78]. In this approach, one evaluates the spin-averaged values of the four Compton scattering diagrams shown in Fig. 2 in terms of the representation

$$
T_{\text{Compton}}^{\text{spin-averaged}} = \hat{\boldsymbol{\epsilon}}_f^* \cdot \hat{\boldsymbol{\epsilon}}_i\, A_1 + \hat{\boldsymbol{\epsilon}}_f^* \cdot \hat{\mathbf{q}}_i\, \hat{\boldsymbol{\epsilon}}_i \cdot \hat{\mathbf{q}}_f\, A_2.
\tag{56}
$$

The results at $\mathcal{O}(q^3)$ can be expressed as a Born plus one-loop contribution

13

[78]

$$A^p_{1,\,\text{Born}} = -\frac{e^2}{m_N}, \quad A^p_{2,\,\text{Born}} = \frac{e^2\omega}{m_N^2},$$

$$A^p_{1,\,\text{loop}} = \frac{e^2 g_A^2 \omega^2}{192\pi F_\pi^2 M_\pi}(10 + \cos\theta), \quad A^p_{2,\,\text{loop}} = -\frac{e^2 g_A^2 \omega^2}{192\pi F_\pi^2 M_\pi}. \tag{57}$$

Using

$$\hat{\boldsymbol{\epsilon}}_f^* \times \hat{\mathbf{q}}_f \cdot \hat{\boldsymbol{\epsilon}}_i \times \hat{\mathbf{q}}_i = \hat{\boldsymbol{\epsilon}}_f^* \cdot \hat{\boldsymbol{\epsilon}}_i \cos\theta - \hat{\boldsymbol{\epsilon}}_f^* \cdot \hat{\mathbf{q}}_i \, \hat{\boldsymbol{\epsilon}}_i \cdot \hat{\mathbf{q}}_f$$

and comparing with the Compton amplitude in Eq. (30), we reproduce the Thomson amplitude and identify the polarizabilities at $\mathcal{O}(q^3)$ as

$$\alpha^p_{E,\text{HB},q^3} = \frac{10\alpha_{\text{em}}g_A^2}{192\pi F_\pi^2 M_\pi} = 12.6 \times 10^{-4}\,\text{fm}^3,$$

$$\beta^p_{M,\text{HB},q^3} = \frac{\alpha_{\text{em}}g_A^2}{192\pi F_\pi^2 M_\pi} = 1.26 \times 10^{-4}\,\text{fm}^3 \tag{58}$$

which reproduces the leading $1/M_\pi$ term in the relativistic ChPT expression of Eq. (55) and agrees quite well with the experimental values of Eq. (35). However, it seems clear that this agreement is somewhat accidental since an $\mathcal{O}(q^4)$ estimate by Bernard, Kaiser, Schmidt, and Meißner yielded the modified values [79, 80]

$$\alpha^p_{E,\text{HB},q^4} = (10.5 \pm 2.0) \times 10^{-4}\,\text{fm}^3 \quad \text{and} \quad \beta^p_{M,\text{HB},q^4} = (3.5 \pm 3.6) \times 10^{-4}\,\text{fm}^3. \tag{59}$$

In particular, the results of Eq. (59) include an estimate of low-energy constants (LECs) entering at $\mathcal{O}(q^4)$. In addition, the inclusion of the $\Delta(1232)$ resonance in either the "small scale expansion" ($\epsilon$ expansion) [81] or the $\delta$ expansion [51, 82] has been shown to make significant modifications to the lowest-order results. In the meantime, the power-counting problem in RChPT has been solved in the framework of *infrared regularization* (IR) [83, 84] and the extended on-mass-shell (EOMS) scheme [85, 86]. Covariant calculations have been performed at next-to-next-to-leading order including the $\Delta(1232)$ resonance [50] and also in the framework of the linear sigma model [87]. In particular, it was stressed in Ref. [50] that the leading-order behavior of the forward-scattering combination ($\alpha^p_E + \beta^p_M$) essentially reflects the Kroll-Ruderman theorem of pion photoproduction [88], whereas the backward-scattering combination ($\alpha^p_E - \beta^p_M$) relies on chiral symmetry. Figure 3 summarizes the present experimental and theoretical situation regarding the scalar polarizabilities of the proton [89].
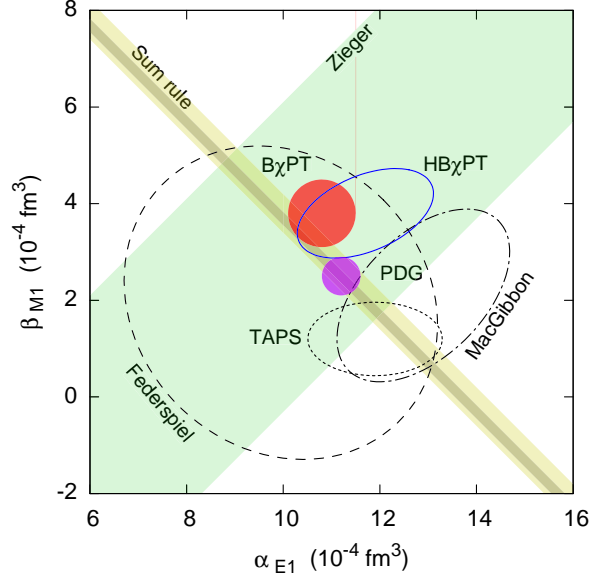
Figure 3: Electric and magnetic polarizabilities $\alpha_{E1}(= \alpha_E^p)$ and $\beta_{M1}(= \beta_M^p)$ of the proton including an updated PDG value [89]. The magenta blob represents the PDG summary of Eq. (35) [26]. The red blob represents the RChPT calculation of Ref. [50] and the blue ellipse the HBChPT calculation of Ref. [51], respectively. Sum rule indicates the Baldin sum rule evaluations of Eq. (42) from Refs. [15] (broad band) and [57] (narrow band), respectively. The experimental results are from Federspiel et al. [11], Zieger et al. [12], MacGibbon et al. [13], and TAPS [15].

## 2.6 Neutron Polarizability

In chiral perturbation theory, the electric and magnetic polarizabilities are expected to be primarily isoscalar quantities, so that the proton and neutron values should be similar. However, on the experimental side, the absence of a neutron target means that the measurement of the neutron polarizabilities is a challenging prospect. Nevertheless, there exist results from a number of approaches.

One technique is to extract the electric polarizability from slow-neutron electromagnetic scattering in the Coulomb field of heavy nuclei, for which the cross section is [6]

$$\frac{d\sigma_{\text{em pol}}}{d\Omega} = 4\pi^2 Z^2 \alpha_{\text{em}} m_n p_n \text{Re}(a) \left[ \alpha_E^n \sin\frac{\theta}{2} - \frac{2\pi\alpha_{\text{em}}\kappa_n^2}{m_n^3} \left( 1 - \sin\frac{\theta}{2} \right) \right], \quad (60)$$

where $p_n$ is the absolute value of the neutron three-momentum, $-a$ is the amplitude for hadronic scattering by the nucleus, $Z$ is the nuclear charge, and $\kappa_n = -1.913$ is the (anomalous) neutron magnetic moment. In this way an experiment at Oak Ridge National Laboratory has yielded a result [16]

$$\alpha_E^n = (12.0 \pm 1.5 \pm 2.0) \times 10^{-4}\,\text{fm}^3, \quad (61)$$

in good agreement with the proton value—Eq. (35). An alternative method to extract the neutron polarizabilities is to utilize quasi-free Compton scattering on the neutron bound in the deuteron, $\gamma d \to \gamma np$, which has given

$$\alpha_E^n = \begin{cases} (10.7^{+3.3}_{-10.7}) \times 10^{-4}\,\text{fm}^3 & [17], \\ (12.5 \pm 2.3) \times 10^{-4}\,\text{fm}^3 & [18], \end{cases} \quad (62)$$

in good agreement with Eq. (61) determined via neutron scattering. This value concurs also with that extracted by the use of coherent Compton scattering from the deuteron, $\alpha_E^n = (8.8 \pm 2.4 \pm 3.0) \times 10^{-4}\,\text{fm}^3$ [19]. The PDG average of the above results is [26]

$$\alpha_E^n = (11.6 \pm 1.5) \times 10^{-4}\,\text{fm}^3. \quad (63)$$

The Baldin sum rule [56] for the neutron has been evaluated to be [58]

$$\alpha_E^n + \beta_M^n = \frac{1}{2\pi^2} \int_0^\infty d\omega \frac{\sigma_{\text{tot}}^n(\omega)}{\omega^2} = (15.2 \pm 0.5) \times 10^{-4}\,\text{fm}^3. \quad (64)$$

16

Using

$$\beta_M^n = \begin{cases} (2.7 \pm 1.8^{+1.3}_{-1.6}) \times 10^{-4}\,\text{fm}^3 & [18], \\ (6.5 \pm 2.4 \pm 3.0) \times 10^{-4}\,\text{fm}^3 & [19], \end{cases} \tag{65}$$

where both determinations make use of the Baldin sum rule, the PDG average is given by [26]

$$\beta_M^n = (3.7 \pm 2.0) \times 10^{-4}\,\text{fm}^3, \tag{66}$$

which is by about 50 % larger than the proton value—Eq. (35)—but also has a larger error bar. We conclude that the electromagnetic polarizabilities $\alpha_E, \beta_M$ are predominantly of isoscalar nature, and that the relative isovector contribution appears to be larger for the magnetic polarizability than for the electric polarizability. For a further discussion of how to extract the neutron polarizabilities see, e.g., Ref. [90] and references therein. Theoretical values have also been predicted for the polarizabilities of the hyperons, but it is unlikely that they will soon be measured [91].

## 2.7 Charged-Pion Polarizability

A good deal of work has also been done involving the charged-pion polarizabilities. In this case, a valence quark picture is not expected to work well since it does not capture the Goldstone nature of the pion. Instead a chiral perturbative technique, wherein the Goldstone nature of the pion *is* exhibited, should be expected to be a reasonable approach and this turns out to be the case [42, 92].

We define the second-rank Compton tensor as

$$T^{\mu\nu}(p_f, q_f; p_i, q_i) = i \int d^4x\, e^{-iq_i \cdot x} \langle \pi^+(p_f)|T[J_{\text{em}}^\mu(x)J_{\text{em}}^\nu(0)]|\pi^+(p_i)\rangle, \tag{67}$$

where $T$ denotes the covariant time-ordered product and $J_{\text{em}}$ is the electromagnetic current operator in units of the elementary charge. Because of translation invariance, four-momentum conservation is implied, $p_f + q_f = p_i + q_i$. For real Compton scattering (RCS), $q_i^2 = q_f^2 = 0$, the one-loop charged-pion tensor is given by [93, 94]

$$\begin{aligned} T_{\text{RCS}}^{\mu\nu} = &-\frac{(2p_f + q_f)^\nu (2p_i + q_i)^\mu}{(p_i + q_i)^2 - M_\pi^2} - \frac{(2p_f - q_i)^\mu (2p_i - q_f)^\nu}{(p_i - q_f)^2 - M_\pi^2} + 2g^{\mu\nu} \\ &+ \zeta \left(q_f^\mu q_i^\nu - g^{\mu\nu} q_i \cdot q_f\right) + \dots, \end{aligned} \tag{68}$$

17

where the first line includes the Born terms while the second line includes the structure dependence. Comparing $T_{\text{RCS}} = e^2 \epsilon_{i\mu} \epsilon_{f\nu}^* T_{\text{RCS}}^{\mu\nu}$ with the definitions for electric, magnetic polarizabilities—Eq. (30)—and noting that the normalization of the covariant expression differs by a factor of $2M_\pi$, we identify

$$\alpha_E^{\pi^+} = -\beta_M^{\pi^+} = \frac{\alpha_{\text{em}}}{2M_\pi}\zeta. \tag{69}$$

That is, at the one-loop level the electric and magnetic polarizabilities are equal and opposite. As for the absolute size, we can relate the polarizability to the axial structure constant $h_A$ in radiative charged-pion beta decay—$\pi^+ \to e^+ \nu_e \gamma$—defined via [95, 96]

$$
\begin{aligned}
A_{\mu\nu}(p, q) &= \int d^4x \, e^{iq \cdot x} \langle 0 \left| T \left( J_\mu^{\text{em}}(x) J_{\nu,1-i2}^{\text{wk}}(0) \right) \right| \pi^+(p) \rangle \\
&= -\sqrt{2} \, F_\pi \frac{(p-q)_\nu}{(p-q)^2 - M_\pi^2} \langle \pi^+(p-q) \left| J_\mu^{\text{em}} \right| \pi^+(p) \rangle + \sqrt{2} \, F_\pi g_{\mu\nu} \\
&\quad - h_A \left[ (p-q)_\mu q_\nu - g_{\mu\nu} q \cdot (p-q) \right] - r_A (q_\mu q_\nu - g_{\mu\nu} q^2) \\
&\quad + i h_V \epsilon_{\mu\nu\alpha\beta} q^\alpha p^\beta.
\end{aligned} \tag{70}
$$

In Eq. (70), the second line is associated with the Born diagram together with a term required for gauge invariance, while the structure-dependent pieces, involving $h_A, r_A, h_V$ appear in the third and fourth lines, with the subscript $V, A$ indicating its connection with the weak vector, axial-vector currents, respectively. (Note that the form factor $r_A$ vanishes for radiative decay to a real photon and only comes into play for the Dalitz decay mode $\pi^+ \to e^+ \nu_e e^+ e^-$.) Chiral symmetry relates $\zeta$ and $h_A$ via [97]

$$
\begin{aligned}
h_V &= \left. \frac{N_c}{12\sqrt{2}\,\pi^2 F_\pi} \right|_{N_c=3}, \\
\frac{h_A}{h_V} &= 32\pi^2 \left( L_9^r(\mu) + L_{10}^r(\mu) \right), \\
\frac{r_A}{h_V} &= 32\pi^2 \left[ L_9^r(\mu) - \frac{1}{192\pi^2} \left( \ln \frac{M_\pi^2}{\mu^2} + 1 \right) \right], \\
\alpha_E^{\pi^+} &= \frac{\alpha_{\text{em}}}{2M_\pi}\zeta = \frac{\alpha_{\text{em}}}{8\pi^2 M_\pi F_\pi^2} \frac{h_A}{h_V}.
\end{aligned} \tag{71}
$$

Here, $h_V$ arises from the anomaly and is exactly predicted at $\mathcal{O}(q^4)$ [98, 99, 100]. The ratio $h_A/h_V$ is given in terms of a linear combination of LECs of

18

the $\mathcal{O}(q^4)$ Lagrangian [92]. The renormalization scale is denoted by $\mu$, but the linear combination $L_9^r(\mu) + L_{10}^r(\mu)$ is scale-independent. The coupling $h_A$ has been measured with great precision by the recent PIBETA experiment [101], resulting in [26]

$$\left(\frac{h_A}{h_V}\right)_{\text{expt}} = 0.469 \pm 0.031 \tag{72}$$

which then corresponds to the one-loop prediction

$$\alpha_E^{\pi^+} = -\beta_M^{\pi^+} = (2.8 \pm 0.2) \times 10^{-4}\,\text{fm}^3. \tag{73}$$

Two-loop corrections are expected to be small by power-counting arguments,

$$\alpha_E^{\pi^+}|_{\text{two-loop}}/\alpha_E^{\pi^+}|_{\text{one-loop}} \sim \frac{4M_\pi^2}{\Lambda_\chi^2} \sim 0.1, \tag{74}$$

where $\Lambda_\chi \sim 4\pi F_\pi$ is the chiral-symmetry-breaking scale [74, 75]. This expectation is borne out by evaluation of the Baldin sum rule [56] for the charged pion, which yields [102]

$$\alpha_E^{\pi^+} + \beta_M^{\pi^+} = \frac{1}{2\pi^2} \int_0^\infty d\omega \frac{\sigma_{\text{tot}}^{\pi^+}(\omega)}{\omega^2} = (0.39 \pm 0.04) \times 10^{-4}\,\text{fm}^3 \tag{75}$$

and by an actual two-loop ChPT calculation [103, 104, 105], which, using updated values for the LECs, yields [105]

$$\begin{aligned}
(\alpha_E^{\pi^+} + \beta_M^{\pi^+})_{\text{two-loop}} &= 0.16 \times 10^{-4}\,\text{fm}^3, \\
(\alpha_E^{\pi^+} - \beta_M^{\pi^+})_{\text{two-loop}} &= (5.7 \pm 1.0) \times 10^{-4}\,\text{fm}^3.
\end{aligned} \tag{76}$$

That the relation Eq. (71) should exist between the pion Compton amplitude and that for axial radiative charged-pion beta decay can be understood from simple current algebra arguments in combination with the hypothesis of a partially conserved axial-vector current [95]—

$$T_{\text{Compton}}^{\mu\nu}(p_2, q_2; p_1, q_1) \xrightarrow{p_2 \to 0} \frac{i}{\sqrt{2}F_\pi} \left(A^{\mu\nu}(p_1, q_1) + A^{\nu\mu}(p_1, q_2)\right). \tag{77}$$

Thus, on the theoretical side we have a rather precise and solid prediction for the charged-pion polarizability and we move to experimental tests.

There have been three different techniques used in the experimental study of the charged-pion polarizability. Since a charged-pion target does not exist, these methods are each indirect and we consider them in turn:

a) The most direct method involves the use of a high-energy pion beam and the $(\pi^+, \pi^+\gamma)$ reaction. Extrapolation to the photon pole using the Primakoff effect then leads to a measurement of the $\gamma\pi^+ \to \gamma\pi^+$ amplitude and thereby the charged-pion polarizability. An experiment by Antipov et al. at Dubna yielded the result [20, 21]

$$\alpha_E^{\pi^+}|_{\text{expt-a1}} = -\beta_M^{\pi^+}|_{\text{expt-a1}} = (6.8 \pm 1.4) \times 10^{-4}\,\text{fm}^3. \qquad (78)$$

A recent experiment by the COMPASS collaboration using the $(\mu^+, \mu^+\gamma)$ reaction as a normalization, has produced a new preliminary number [25]

$$\alpha_E^{\pi^+}|_{\text{expt-a2}} = -\beta_M^{\pi^+}|_{\text{expt-a2}} = (1.9 \pm 0.7 \pm 0.8) \times 10^{-4}\,\text{fm}^3. \qquad (79)$$

b) An alternative way to access the pion Compton amplitude is via the radiative pion photoproduction reaction $\gamma p \to \gamma n\pi^+$. The analysis of a measurement by Aibergenov et al. [22] at the Lebedev Physical Institute made use of an extrapolation to the pion pole at $t = M_\pi^2$ in the unphysical region, yielding the number

$$\alpha_E^{\pi^+}|_{\text{expt-b1}} = -\beta_M^{\pi^+}|_{\text{expt-b1}} = (20 \pm 12) \times 10^{-4}\,\text{fm}^3. \qquad (80)$$

A different approach avoiding an extrapolation was chosen in the analysis of the more recent experiment at the Mainz Microtron (MAMI) [24]. The $\pi^+$ polarizabilities have been determined from a comparison of the data with the predictions of two different theoretical models:

$$(\alpha_E^{\pi^+} - \beta_M^{\pi^+})|_{\text{expt-b2}} = (11.6 \pm 1.5_{\text{stat}} \pm 3.0_{\text{syst}} \pm 0.5_{\text{mod}}) \times 10^{-4}\,\text{fm}^3. \qquad (81)$$

c) A direct measurement via the $\gamma\gamma \to \pi^+\pi^-$ reaction at SLAC has yielded the result [23]

$$\alpha_E^{\pi^+}|_{\text{expt-c}} = -\beta_M^{\pi^+}|_{\text{expt-c}} = (2.2 \pm 1.1) \times 10^{-4}\,\text{fm}^3. \qquad (82)$$

There is thus considerable experimental uncertainty at the present time and additional experimental work in this regard is urgently needed in order to confirm these presumably solid chiral perturbative predictions. An approved JLab experiment using the Primakoff effect and the $(\gamma, \pi^+\pi^-)$ reaction should be helpful in this regard [106].

## 2.8 Neutral-Pion and Kaon Polarizabilities

There has also been a substantial amount of work on neutral-pion pair production in two-photon collisions. Data were taken by the Crystal Ball Collaboration for $\pi^0\pi^0$ invariant masses $W$ from threshold to 2 GeV [107] and, more recently, by the Belle Collaboration [108] in the kinematic range 0.6 GeV $\leq W \leq$ 4.0 GeV. At the one-loop level, ChPT makes a parameter-free prediction for the neutral-pion polarizabilities [93, 94, 109]:

$$\alpha_E^{\pi^0} = -\beta_M^{\pi^0} = -\frac{\alpha_{\text{em}}}{96\pi^2 F_\pi^2 M_\pi} = -0.5 \times 10^{-4}\,\text{fm}^3. \tag{83}$$

Note in particular that the electric polarizability is negative. Two-loop calculations of the $\gamma\gamma \to \pi^0\pi^0$ reaction have been performed in Refs. [110, 111, 112] and, using updated values for the LECs, the two-loop results for the sum and the difference of polarizabilities are given by [112]

$$\begin{aligned}
(\alpha_E^{\pi^0} + \beta_M^{\pi^0})_{\text{two-loop}} &= (1.1 \pm 0.3) \times 10^{-4}\,\text{fm}^3, \\
(\alpha_E^{\pi^0} - \beta_M^{\pi^0})_{\text{two-loop}} &= -(1.9 \pm 0.2) \times 10^{-4}\,\text{fm}^3.
\end{aligned} \tag{84}$$

As in the case of the charged pions, the degeneracy $\alpha_E^{\pi^0} + \beta_M^{\pi^0} = 0$ is lifted at the two-loop level. For a discussion of quadrupole polarizabilities see, e.g., Refs. [112, 113]. Recent dispersion-theoretical treatments of the $\gamma\gamma \to \pi\pi$ reaction can be found in [113, 114, 115, 116].

The one-loop predictions for the charged-kaon polarizabilities are determined by the same linear combination of LECs as those of the charged-pion polarizabilities. One simply needs to replace the pion mass and pion-decay constant by the kaon mass and kaon-decay constant, respectively [117]:

$$\alpha_E^{K^+} = -\beta_M^{K^+} = 4\frac{\alpha_{\text{em}}}{F_K^2 M_K}\left(L_9^r(\mu) + L_{10}^r(\mu)\right) = 0.58 \times 10^{-4}\,\text{fm}^3, \tag{85}$$

while the neutral-kaon polarizabilities vanish at this order [118]. Unfortunately, except for an upper limit $|\alpha_E^{K^-}| < 200 \times 10^{-4}\,\text{fm}^3$ from kaonic atoms [119], no experimental information on kaon polarizabilities is available, though in principle, the charged-kaon polarizabilities could also be investigated by the COMPASS collaboration via the Primakoff reaction with a kaon beam [120].

# 3 Spin Polarizabilities

As emphasized above, in a low-energy expansion the leading—$\mathcal{O}(\omega^2)$—correction to the Thomson amplitude is given by the spin-independent (scalar) electric and magnetic polarizability terms given in Eq. (29). At higher—$\mathcal{O}(\omega^3)$—order there exist four additional—*spin-dependent*—forms (spin polarizabilities) as first pointed out by Ragusa [30, 31], which can be written in the form [32]

$$
\begin{aligned}
H_{\mathrm{eff}}^{(3)} = -\frac{1}{2}4\pi \Big( & \gamma_{E1E1}\,\boldsymbol{\sigma}\cdot\mathbf{E}\times\dot{\mathbf{E}} + \gamma_{M1M1}\,\boldsymbol{\sigma}\cdot\mathbf{H}\times\dot{\mathbf{H}} \\
& + 2\gamma_{E1M2}\,\sigma_i E_j H_{ij} - 2\gamma_{M1E2}\,\sigma_i H_j E_{ij} \Big),
\end{aligned}
\tag{86}
$$

where $E_{ij}, H_{ij} = \frac{1}{2}(\nabla_i E_j + \nabla_j E_i), \frac{1}{2}(\nabla_i H_j + \nabla_j H_i)$ are field gradients and the subscripts on the spin polarizabilities indicate the associated excitation/deexcitation photon multipolarities. In this case there is no simple classical analogy in order to understand the significance of the spin polarizabilities. The Compton scattering amplitude can be written in the spin-dependent form

$$
\begin{aligned}
T_{\mathrm{RCS}} = &\,\hat{\boldsymbol{\epsilon}}_f^*\cdot\hat{\boldsymbol{\epsilon}}_i\,A_1 + \hat{\boldsymbol{\epsilon}}_f^*\cdot\hat{\mathbf{q}}_i\,\hat{\boldsymbol{\epsilon}}_i\cdot\hat{\mathbf{q}}_f\,A_2 + i\boldsymbol{\sigma}\cdot(\hat{\boldsymbol{\epsilon}}_f^*\times\hat{\boldsymbol{\epsilon}}_i)A_3 \\
& + i\boldsymbol{\sigma}\cdot(\hat{\mathbf{q}}_f\times\hat{\mathbf{q}}_i)\hat{\boldsymbol{\epsilon}}_f^*\cdot\hat{\boldsymbol{\epsilon}}_i A_4 + i\boldsymbol{\sigma}\cdot[(\hat{\boldsymbol{\epsilon}}_f^*\times\hat{\mathbf{q}}_i)\hat{\boldsymbol{\epsilon}}_i\cdot\hat{\mathbf{q}}_f - (\hat{\boldsymbol{\epsilon}}_i\times\hat{\mathbf{q}}_f)\hat{\boldsymbol{\epsilon}}_f^*\cdot\hat{\mathbf{q}}_i]A_5 \\
& + i\boldsymbol{\sigma}\cdot[(\hat{\boldsymbol{\epsilon}}_f^*\times\hat{\mathbf{q}}_f)\hat{\boldsymbol{\epsilon}}_i\cdot\hat{\mathbf{q}}_f - (\hat{\boldsymbol{\epsilon}}_i\times\hat{\mathbf{q}}_i)\hat{\boldsymbol{\epsilon}}_f^*\cdot\hat{\mathbf{q}}_i]A_6
\end{aligned}
\tag{87}
$$

with

$$
A_i = A_i^{\mathrm{Born}} + A_i^{\mathrm{non\text{-}Born}}.
\tag{88}
$$

Here the Born amplitudes are given by (with the superscript $p$ omitted for notational reasons)

$$
A_1^{\mathrm{Born}} = -\frac{e^2}{m_p}, \quad A_2^{\mathrm{Born}} = \frac{e^2\omega}{m_p^2}, \quad A_3^{\mathrm{Born}} = \frac{e^2\omega}{2m_p^2}\left[1 + 2\kappa_p - (1+\kappa_p)^2\cos\theta\right],
$$

$$
A_4^{\mathrm{Born}} = -A_5^{\mathrm{Born}} = -\frac{e^2\omega(1+\kappa_p)^2}{2m_p^2}, \quad A_6^{\mathrm{Born}} = -\frac{e^2\omega(1+\kappa_p)}{2m_p^2},
\tag{89}
$$

where $\kappa_p = 1.793$ is the proton anomalous magnetic moment in units of the nuclear magneton. Equation (89) agrees with the predictions of the low-energy theorem of real Compton scattering on a spin-1/2 target [121, 122],

22

while the structure-dependent counterparts from Eq. (86) are

$$A_1^{\text{non-Born}} = 4\pi(\alpha_E + \beta_M \cos\theta)\omega^2 + \mathcal{O}(\omega^3),$$
$$A_2^{\text{non-Born}} = -4\pi\beta_M\omega^2 + \mathcal{O}(\omega^3),$$
$$A_3^{\text{non-Born}} = -4\pi[\gamma_{E1E1} + \gamma_{E1M2} + (\gamma_{M1M1} + \gamma_{M1E2})\cos\theta]\omega^3 + \mathcal{O}(\omega^4),$$
$$A_4^{\text{non-Born}} = -4\pi(\gamma_{M1M1} - \gamma_{M1E2})\omega^3 + \mathcal{O}(\omega^4),$$
$$A_5^{\text{non-Born}} = 4\pi\gamma_{M1M1}\omega^3 + \mathcal{O}(\omega^4),$$
$$A_6^{\text{non-Born}} = 4\pi\gamma_{E1M2}\omega^3 + \mathcal{O}(\omega^4). \tag{90}$$

However, there exists a significant contribution to each spin polarizability from the $t$-channel pion-pole diagram which carries no new information about nucleon structure,

$$\gamma_{E1E1}^{\pi\text{-pole}} = -\gamma_{M1M1}^{\pi\text{-pole}} = \gamma_{E1M2}^{\pi\text{-pole}} = -\gamma_{M1E2}^{\pi\text{-pole}} = \frac{\alpha_{\text{em}}g_A}{8\pi^2 F_\pi^2 M_\pi^2} = 10.7 \times 10^{-4}\,\text{fm}^4. \tag{91}$$

The structure-dependent pieces of the spin polarizabilities are then given by subtracting these pole contributions

$$\gamma_i^{\text{structure}} = \gamma_i - \gamma_i^{\pi\text{-pole}}. \tag{92}$$

In one-loop chiral perturbation theory we determine the $\mathcal{O}(q^3)$ predictions [71, 123]

$$\gamma_{E1E1}^{\text{structure}} = -5\gamma_{M1M1}^{\text{structure}} = 5\gamma_{E1M2}^{\text{structure}} = 5\gamma_{M1E2}^{\text{structure}}$$
$$= -\frac{\alpha_{\text{em}}g_A^2}{192\pi^2 F_\pi^2 M_\pi^2} = -0.569 \times 10^{-4}\,\text{fm}^4 \tag{93}$$

which are much smaller than the corresponding pion-pole contributions. Full one-loop calculations to $\mathcal{O}(q^4)$ have been performed in Refs. [124, 125]. No new LECs, except for the anomalous magnetic moments of the nucleon, enter at this order, but the degeneracy between proton and neutron polarizabilities is lifted. Unfortunately, the next-to-leading-order contributions turn out to be very large, calling the convergence of the expansion into question [125]. Various theoretical predictions for the spin-dependent polarizabilities of the proton are summarized in Table 2.

At the present time there exists no direct determination of the four spin polarizabilities from Compton scattering, though there are existing programs

Table 2: Theoretical predictions for the *structure-dependent* contribution to the spin polarizabilities of the proton to $\mathcal{O}(q^3)$ in HBChPT, to $\mathcal{O}(q^4)$ in HBChPT from two derivations, to $\mathcal{O}(\varepsilon^3)$ in the small-scale expansion, in fixed-$t$ dispersion relation analyses (BGLMN) and (HDPV), in a calculation with hyperbolic dispersion relations (HYP. DR) at $\theta_{\text{lab}} = 180^\circ$, in a dressed $K$-matrix model (KS), and from chiral dynamics with unitarity and causality (GLP). The values are given in units of $10^{-4}$ fm$^4$. Here $\gamma_0^p$ and $\gamma_\pi^p$ are the combinations relevant for forward and backward scattering and are defined in Eqs. (96) and (102).

|  | $\gamma_{E1E1}^p$ | $\gamma_{M1M1}^p$ | $\gamma_{E1M2}^p$ | $\gamma_{M1E2}^p$ | $\gamma_0^p$ | $\gamma_\pi^p$ |
|---|---|---|---|---|---|---|
| $\mathcal{O}(q^3)$ [71, 123] | $-5.7$ | $-1.1$ | $1.1$ | $1.1$ | $4.6$ | $4.6$ |
| $\mathcal{O}(q^4)$ [124] | $-1.8$ | $0.4$ | $0.7$ | $1.8$ | $-1.1$ | $3.3$ |
| $\mathcal{O}(\varepsilon^3)$ [124] | $-5.4$ | $1.4$ | $1.0$ | $1.0$ | $2.0$ | $6.8$ |
| $\mathcal{O}(q^4)$ [125] | $-1.4$ | $3.3$ | $0.2$ | $1.8$ | $-3.9$ | $6.3$ |
| BGLMN [32] | $-3.4$ | $2.7$ | $0.3$ | $1.9$ | $-1.5$ | $7.8$ |
| HDPV [33] | $-4.3$ | $2.9$ | $-0.01$ | $2.1$ | $-0.7$ | $9.3$ |
| HYP. DR [8] | $-3.8$ | $2.9$ | $0.5$ | $1.6$ | $-1.1$ | $7.8$ |
| KS [126] | $-5.0$ | $3.4$ | $-1.8$ | $1.1$ | $2.4$ | $11.4$ |
| GLP [127] | $-3.7$ | $2.5$ | $1.2$ | $1.2$ | $-1.2$ | $6.1$ |

for such measurements at MAMI and at the High Intensity Gamma-Ray Source (HIGS) at Duke University. However, there are two different determinations of various combinations, one which is relevant in the case of forward Compton scattering and the second which applies to backward scattering.

We begin with the forward case. In order to see how this constraint comes about consider the general amplitude for forward Compton scattering from the nucleon—Eq. (37). Here the dispersion relation involving the spin-independent amplitude $f_0(\omega)$ was given above, while that for the corre-

sponding spin-dependent amplitude $g_0(\omega)$ is [54]

$$\mathrm{Re}\left[g_0(\omega)\right] = \frac{\omega}{4\pi^2} P \int_0^\infty d\omega' \frac{\omega'}{\omega'^2 - \omega^2} \left(\sigma_{1/2}(\omega') - \sigma_{3/2}(\omega')\right), \qquad (94)$$

where $\sigma_{3/2}(\omega'), \sigma_{1/2}(\omega')$ are the photoabsorption cross sections in the case that the incident photon helicity is parallel, antiparallel to the target spin, respectively, and, since there is a spin flip involved, the dispersion relation does *not* require a subtraction. The spin-dependent component of the proton forward Compton amplitude is given by

$$g_0^p(\omega) = -\frac{e^2 \kappa_p^2}{8\pi m_p^2} \omega + \gamma_0^p \omega^3 + \dots, \qquad (95)$$

where

$$\gamma_0 = -\gamma_{E1E1} - \gamma_{M1M1} - \gamma_{E1M2} - \gamma_{M1E2} \qquad (96)$$

is the combination of spin polarizabilities relevant for forward Compton scattering. Note that the pion-pole contribution cancels out in the forward direction, so that only structure-dependent components remain. Equating the two forms for the spin-flip amplitude we find two sum rules. One is for the anomalous magnetic moment and is the well-known Gerasimov-Drell-Hearn (GDH) sum rule [128, 129]

$$\frac{2\pi^2 \alpha_{\mathrm{em}} \kappa_p^2}{m_p^2} = \int_0^\infty \frac{d\omega}{\omega} \left(\sigma_{3/2}^p(\omega) - \sigma_{1/2}^p(\omega)\right) \equiv I_{\mathrm{GDH}}^p \qquad (97)$$

and the second is a sum rule for the forward spin polarizability

$$\gamma_0^p = -\frac{1}{4\pi^2} \int_0^\infty \frac{d\omega}{\omega^3} \left(\sigma_{3/2}^p(\omega) - \sigma_{1/2}^p(\omega)\right). \qquad (98)$$

The numerical value of the LHS of Eq. (97) is 204.8 $\mu$b. The GDH collaboration has measured the cross section difference $(\sigma_{3/2}^p - \sigma_{1/2}^p)$ in the photon energy range from 0.2 to 2.9 GeV with the tagged photon facilities at MAMI (Mainz) and ELSA (Bonn) [130, 131, 132, 133]. Using theoretical input for the energy regions below $\omega = 0.2$ GeV and above $\omega = 2.9$ GeV, the total RHS result was determined to be [134] (see Table 3)

$$I_{\mathrm{GDH}}^p = (211 \pm 15)\,\mu\mathrm{b}, \qquad (99)$$

25

Table 3: Contribution of various energy regions to the GDH integral $I^p_{\mathrm{GDH}}$ and the forward spin polarizability $\gamma^p_0$ of the proton

| Energy range | $I^p_{\mathrm{GDH}}$ [$\mu$b] | $\gamma^p_0$ [$10^{-4}$ fm$^4$] |
|---|---|---|
| $\omega \leq 200$ MeV [135, 136] | $-28.5 \pm 2$ | $0.95 \pm 0.05$ |
| 200 MeV$\leq \omega \leq 800$ MeV [131] | $226 \pm 5 \pm 12$ | $-1.87 \pm 0.08 \pm 0.10$ |
| 800 MeV$\leq \omega \leq 2.9$ GeV [133] | $27.5 \pm 2.0 \pm 1.2$ | $-0.03$ |
| $\omega \geq 2.9$ GeV [137, 138] | $-14 \pm 2$ | $+0.01$ |
| Total | $211 \pm 15$ | $-0.94 \pm 0.15$ |
| Sum rule [128, 129] | $204.8$ | $-$ |

so that the proton GDH sum rule is satisfied. The sum rule for the forward spin polarizability then becomes [134] (see Table 3)

$$\gamma_0^{p\text{-sum-rule}} = (-0.94 \pm 0.15) \times 10^{-4}\,\mathrm{fm}^4 \tag{100}$$

which is in strong disagreement with the one-loop HBChPT prediction—

$$\gamma_0^{p\text{-one-loop}} = \frac{\alpha_{\mathrm{em}}g_A^2}{24\pi^2 F_\pi^2 M_\pi^2} = 4.55 \times 10^{-4}\,\mathrm{fm}^4 \tag{101}$$

so that there must exist a significant contribution from higher-order terms.

In the backward direction there exists a different combination of spin polarizabilities which is relevant

$$\gamma_\pi = -\gamma_{E1E1} + \gamma_{M1M1} - \gamma_{E1M2} + \gamma_{M1E2} \tag{102}$$

and this backward spin polarizability has been determined experimentally from a global fit to Compton scattering [9]

$$\gamma_\pi^{p\text{-exp}} = -(38.7 \pm 1.8) \times 10^{-4}\,\mathrm{fm}^4. \tag{103}$$

Note that in this case the pion pole *does* contribute

$$\gamma_\pi^{p\text{-}\pi^0\text{-pole}} = -\frac{\alpha_{\mathrm{em}}g_A}{2\pi^2 F_\pi^2 M_\pi^2} = -42.8 \times 10^{-4}\,\mathrm{fm}^{-4}. \tag{104}$$

26

The difference between Eqs. (103) and (104) is then the structure component of the backward spin polarizability and is much smaller than the pion-pole piece

$$\gamma_\pi^{p\text{-structure}} = (4.0 \pm 1.8) \times 10^{-4}\,\text{fm}^4. \tag{105}$$

In this case the one-loop—$\mathcal{O}(q^3)$—chiral prediction is found to be

$$\gamma_\pi^{p\text{-one-loop}} = \frac{\alpha_{\text{em}} g_A^2}{160\pi^2 F_\pi^2 M_\pi^2} = 0.683 \times 10^{-4}\,\text{fm}^4. \tag{106}$$

At the present time, the only reliable data which is available is that for the forward and backward spin polarizabilities. However, in the near future this situation will change substantially due to Compton scattering experiments involving polarized photons and polarized targets. This effort should take place at MAMI, where such work has already begun and at HIGS, where improved mirrors should enable a viable future program. At MAMI, a series of measurements is envisioned in the photon energy range of about 80-300 MeV and is of three types:

a) Linearly polarized photons either parallel or perpendicular to the scattering plane with an unpolarized target (usually called the beam asymmetry):

$$\Sigma_3 = \frac{\sigma_\parallel - \sigma_\perp}{\sigma_\parallel + \sigma_\perp}. \tag{107}$$

b) Circularly polarized photons and target spin aligned longitudinally with the beam direction:

$$\Sigma_{2z} = \frac{\sigma_{+z}^R - \sigma_{+z}^L}{\sigma_{+z}^R + \sigma_{+z}^L} = \frac{\sigma_{+z}^R - \sigma_{-z}^R}{\sigma_{+z}^R + \sigma_{-z}^R}. \tag{108}$$

c) Circularly polarized photons and target spin aligned transverse to the beam direction:

$$\Sigma_{2x} = \frac{\sigma_{+x}^R - \sigma_{+x}^L}{\sigma_{+x}^R + \sigma_{+x}^L} = \frac{\sigma_{+x}^R - \sigma_{-x}^R}{\sigma_{+x}^R + \sigma_{-x}^R}. \tag{109}$$

Here the measurements of $\Sigma_{2x}$ and $\Sigma_3$ have already been accomplished, while the remaining measurement of $\Sigma_{2z}$ is scheduled to take place in 2014 [139]. Analysis of the $\Sigma_{2x}$ data has already led to a preliminary value for $\gamma_{E1E1}^p = (-4.3 \pm 1.5) \times 10^{-4}\,\text{fm}^4$ [140], the data on $\Sigma_3$ are presently analyzed, and the remaining data should enable determination of the other spin polarizabilities.

27

# 4 Higher-Order Polarizabilities

It is obvious that the concept of polarizabilities can be generalized to even higher orders [33] (see also Refs. [141, 142] for a definition of so-called dynamical polarizabilities). For example, in the spin-independent sector the $\mathcal{O}(\omega^4)$ generalization of the effective Hamiltonian can be written as [32]

$$H_{\text{eff}}^{(4)} = -\frac{1}{2} 4\pi \alpha_{E\nu} \dot{\mathbf{E}}^2 - \frac{1}{2} 4\pi \beta_{M\nu} \dot{\mathbf{H}}^2 - \frac{1}{12} 4\pi \alpha_{E2} E_{ij}^2 - \frac{1}{12} 4\pi \beta_{M2} H_{ij}^2. \quad (110)$$

The meaning of these new quadratic terms is clear. The quantities $\alpha_{E\nu}$ and $\beta_{M\nu}$ represent dispersive corrections to the leading electric and magnetic polarizabilities and measure the frequency dependence of the electric and magnetic polarizabilities via

$$\begin{aligned}
\mathbf{p}(\omega) &= 4\pi(\alpha_E + \alpha_{E\nu}\omega^2 + \ldots)\mathbf{E}(\omega), \\
\mathbf{m}(\omega) &= 4\pi(\beta_M + \beta_{M\nu}\omega^2 + \ldots)\mathbf{H}(\omega).
\end{aligned} \quad (111)$$

Likewise, it is clear that the quadrupole polarizabilities $\alpha_{E2}$ and $\beta_{M2}$ measure the size of the induced quadrupole moments in the presence of an applied field gradient via

$$\begin{aligned}
Q_{ij} &= -\frac{\partial H_{\text{eff}}^{(4)}}{\partial E_{ij}} = \frac{1}{6} 4\pi \alpha_{E2} E_{ij}, \\
M_{ij} &= -\frac{\partial H_{\text{eff}}^{(4)}}{\partial H_{ij}} = \frac{1}{6} 4\pi \alpha_{M2} H_{ij},
\end{aligned} \quad (112)$$

where

$$Q_{ij} = \langle \psi | \sum_{k=1}^{3} q_k \left[ 3(r_k - R)_i (r_k - R)_j - \delta_{ij} (\mathbf{r}_k - \mathbf{R})^2 \right] | \psi \rangle \quad (113)$$

is the induced electric quadrupole moment and $M_{ij}$ is its magnetic analog.

These four new polarizabilities can be calculated in various pictures of the nucleon. For example, in the simple harmonic oscillator picture the sum rules

$$\alpha_{E\nu}^p = 2\alpha_{\text{em}} \sum_{n \neq 0} \frac{|\langle n | D_z | 0 \rangle_p|^2}{(E_n - E_0)^3}, \quad \alpha_{E2}^p = \frac{\alpha_{\text{em}}}{2} \sum_{n \neq 0} \frac{|\langle n | Q_{33} | 0 \rangle_p|^2}{E_n - E_0} \quad (114)$$

yield the predictions

$$\alpha_{E\nu}^p = \frac{2\alpha_{\text{em}}m_p^3}{81}\langle (r_E^p)^2\rangle^4, \quad \alpha_{E2}^p = \frac{\alpha_{\text{em}}m_p}{9}\langle (r_E^p)^2\rangle^3 \tag{115}$$

and similarly the magnetic polarizabilities can be estimated. Introducing

$$\xi_1 = \frac{\alpha_{\text{em}}g_A^2}{1920\,\pi F_\pi^2 M_\pi^3} = 2.53 \times 10^{-5}\,\text{fm}^5,$$

the one-loop $[\mathcal{O}(q^3)]$ HBChPT predictions of these quantities for the proton/neutron read [123]

$$\alpha_{E\nu} = 9\,\xi_1, \quad \beta_{M\nu} = 14\,\xi_1, \quad \alpha_{E2} = 84\,\xi_1, \quad \beta_{M2} = -36\,\xi_1 \tag{116}$$

and the $\Delta$-resonance corrections have also been given in the small-scale expansion [33].

Likewise, in the case that spin dependence is considered, there exist eight new spin polarizabilities which arise at $\mathcal{O}(\omega^5)$—

$$\begin{aligned}
H_{\text{eff}}^{(5)} = -\frac{1}{2}4\pi\Big[&\gamma_{E1\nu}\boldsymbol{\sigma}\cdot\dot{\mathbf{E}}\times\ddot{\mathbf{E}} + \gamma_{M1\nu}\boldsymbol{\sigma}\cdot\dot{\mathbf{H}}\times\ddot{\mathbf{H}} \\
&- 2\gamma_{E2\nu}\sigma_i\dot{E}_{ij}H_j + 2\gamma_{M2\nu}\sigma_i\dot{H}_{ij}E_j \\
&+ 4\gamma_{ET}\epsilon_{ijk}\sigma_i E_{jl}\dot{E}_{kl} + 4\gamma_{MT}\epsilon_{ijk}\sigma_i\dot{H}_{jl}H_{kl} \\
&- 6\gamma_{E3}\sigma_i E_{ijk}H_{jk} + 6\gamma_{M3}\sigma_i H_{ijk}E_{jk}\Big],
\end{aligned} \tag{117}$$

where

$$E_{ijk} = \frac{1}{3}(\nabla_i\nabla_j E_k + \nabla_i\nabla_k E_j + \nabla_j\nabla_k E_i) - \frac{1}{15}(\delta_{ij}\nabla^2 E_k + \delta_{ik}\nabla^2 E_j + \delta_{jk}\nabla^2 E_i) \tag{118}$$

with a corresponding expression for $H_{ijk}$. Again we can identify the one-loop heavy-baryon chiral predictions [33]

$$\begin{aligned}
\gamma_{E3} = 20\,\xi_2, \quad \gamma_{M3} = 20\,\xi_2, \quad \gamma_{ET} = -65\,\xi_2, \quad \gamma_{MT} = -5\xi_2, \\
\gamma_{E1\nu} = -945\,\xi_2, \quad \gamma_{M1\nu} = -45\,\xi_2, \quad \gamma_{E2\nu} = 78\,\xi_2, \quad \gamma_{M2\nu} = -42\,\xi_2,
\end{aligned} \tag{119}$$

where

$$\xi_2 = \frac{\alpha_{\text{em}}g_A^2}{43200\,\pi^2 F_\pi^2 M_\pi^4} = 5.05 \times 10^{-7}\,\text{fm}^6.$$

However, again there is an anomaly contribution which should be subtracted (added) in the proton (neutron) case from the measured value to yield the structure dependence

$$\gamma_{E3}^{\pi\text{-pole}} = -10\,\xi_3, \quad \gamma_{M3}^{\pi\text{-pole}} = 10\,\xi_3, \quad \gamma_{ET}^{\pi\text{-pole}} = 5\,\xi_3, \quad \gamma_{MT}^{\pi\text{-pole}} = -5\,\xi_3,$$
$$\gamma_{E1\nu}^{\pi\text{-pole}} = -45\,\xi_3, \quad \gamma_{M1\nu}^{\pi\text{-pole}} = 45\,\xi_3, \quad \gamma_{E2\nu}^{\pi\text{-pole}} = 46\,\xi_3, \quad \gamma_{M2\nu}^{\pi\text{-pole}} = -46\,\xi_3,$$
$$(120)$$

where
$$\xi_3 = \frac{\alpha_{\text{em}} g_A}{120\,\pi^2 F_\pi^2 M_\pi^4} = 1.43 \times 10^{-4}\,\text{fm}^6.$$

There exist two reliable determinations of combinations of these quantities, which can be compared directly with experiment. These arise from the use of forward dispersion relations. In the case of the spin-independent polarizabilities we find [32]

$$\alpha_{E\nu}^p + \beta_{M\nu}^p + \frac{1}{12}\left(\alpha_{E2}^p + \beta_{M2}^p\right) = \frac{1}{4\pi^2} \int_0^\infty \frac{d\omega}{\omega^4}\left(\sigma_{3/2}^p(\omega) + \sigma_{1/2}^p(\omega)\right)$$
$$= 5.73 \times 10^{-4}\,\text{fm}^5 \tag{121}$$

to be compared with the $\mathcal{O}(q^3)$ chiral prediction

$$\left[\alpha_{E\nu}^p + \beta_{M\nu}^p + \frac{1}{12}\left(\alpha_{E2}^p + \beta_{M2}^p\right)\right]_{\text{HB},q^3} = 27\,\zeta_1 = 6.83 \times 10^{-4}\,\text{fm}^5, \tag{122}$$

while in the case of the spin-polarizabilities, we have [143]

$$-\left(\gamma_{E1\nu}^p + \gamma_{M1\nu}^p + \gamma_{E2\nu}^p + \gamma_{M2\nu}^p + \frac{8}{5}\gamma_{E3}^p + \frac{8}{5}\gamma_{M3}^p + \gamma_{ET}^p + \gamma_{MT}^p\right)$$
$$= -\frac{1}{4\pi^2} \int_0^\infty \frac{d\omega}{\omega^5}\left(\sigma_{3/2}^p(\omega) - \sigma_{1/2}^p(\omega)\right)$$
$$= (0.42 \pm 0.09 \pm 0.09) \times 10^{-4}\,\text{fm}^6 \tag{123}$$

to be compared with the $\mathcal{O}(q^3)$ chiral prediction

$$-\left(\gamma_{E1\nu}^p + \gamma_{M1\nu}^p + \gamma_{E2\nu}^p + \gamma_{M2\nu}^p + \frac{8}{5}\gamma_{E3}^p + \frac{8}{5}\gamma_{M3}^p + \gamma_{ET}^p + \gamma_{MT}^p\right)_{\text{HB},q^3}$$
$$= 960\,\zeta_2 = 4.85 \times 10^{-4}\,\text{fm}^6. \tag{124}$$

However, separating the various polarizabilities is more difficult. While in principle the individual higher-order polarizabilities can be determined from analysis of experimental data, in practice this is not feasible. The problem is that the effective action picture is an expansion in powers of $\omega/\Lambda_\chi$, where $\Lambda_\chi \sim 4\pi F_\pi$ is the chiral scale. As discussed above, at the lowest energies, the cross section is determined simply by the Born terms and is given by the Powell cross section. In the region 50 MeV$\leq \omega \leq$ 100 MeV the dipole polarizabilities come into play and it is this region which has been used in the experimental determination of these quantities. Even at these relatively low energies, however, there are important contributions from the higher-order terms and these must be estimated (usually dispersively) in order to perform the experimental extraction of $\alpha_E^p, \beta_M^p$. This problem is exacerbated at higher energies so that it is not realistic to think that one can extract quadrupole polarizabilities or higher in this fashion.

It *is*, however, possible to make an experimental determination by *indirect* means. That is, one can use subtracted fixed-$t$ dispersion relations to provide a complete low-energy analysis of the Compton amplitude and then to extract the relevant polarizabilities from this calculated amplitude. In this approach, one writes each invariant amplitude $A_i(\nu, t)$ in the form [41]

$$\text{Re}[A_i(\nu,t)] = A_i^{\text{Born}}(\nu,t) + [A_i(0,t) - A_i^{\text{Born}}(0,t)] + \frac{2\nu^2}{\pi} P \int_{\nu_0}^{\infty} d\nu' \frac{\text{Im}_s[A_i(\nu',t)]}{\nu'(\nu'^2 - \nu^2)},$$
(125)

where $\nu = (s - u)/4m_N$ is the average of the incoming and outgoing photon energy—$\nu = \frac{1}{2}(E_\gamma + E_\gamma')$—and $\text{Im}_s[A_i]$ denotes the discontinuities across the $s$-channel cuts of the Compton process. Because of the three powers of $\nu'$ in the denominator, these subtracted dispersion relations should converge and moreover, they should be dominated by the contribution of the $\pi N$ intermediate state, which can be well-determined by experiment. Contributions from states with more than a single pion are expected to be small and can be estimated in simple models. The one unknown in Eq. (125) is the value $A_i(0,t)$ which is determined via a subtracted dispersion relation in $t$,

$$A_i(0,t) = A_i^{\text{Born}}(0,t) + [A_i(0,0) - A_i^{\text{Born}}(0,0)] + [A_i^{t\text{-pole}}(0,t) - A_i^{t\text{-pole}}(0,0)]$$

$$+ \frac{t}{\pi} \int_{4M_\pi^2}^{\infty} dt' \frac{\text{Im}_t[A_i(0,t')]}{t'(t'-t)} - \frac{t}{\pi} \int_{-\infty}^{-2M_\pi^2 - 4M_\pi m_N} dt' \frac{\text{Im}_t[A_i(0,t')]}{t'(t'-t)},$$
(126)

where $A_i^{t\text{-pole}}(0,t)$ represents the contribution from $t$-channel poles, including

31

the $\pi^0$ pole that we have discussed above. The imaginary component of the amplitudes $A_i(0, t)$ in the integral from $4M_\pi^2$ to $\infty$ is estimated by assuming saturation by light intermediate states such as $\pi\pi$ and $K\bar{K}$, while that in the integral from $-\infty$ to $-2M_\pi^2 - 4M_\pi m_N$ is estimated by assuming saturation by the $\Delta$ resonance plus small nonresonant $\pi N$ contributions. In this fashion, the six invariant amplitudes have been determined in terms of the six subtraction constants $A_i(0, 0)$. Four of these constants are evaluated via unsubtracted $t = 0$ dispersion relations

$$A_i(0, 0) = \frac{2}{\pi} \int_{\nu_0}^{\infty} d\nu \frac{\text{Im}[A_i(\nu, 0)]}{\nu}, \quad i = 3, 4, 5, 6, \tag{127}$$

and the remaining two constants are determined from experiment, in terms of the constants $(\alpha_E^p - \beta_M^p)$ and $\gamma_\pi^p$. With the Compton amplitude now determined, the various polarizabilities can now be found and compared to chiral predictions, as shown below. In the case of the quadrupole spin-independent polarizabilities, we find [33]

$$\alpha_{E2}^p = 29.31 \times 10^{-4} \, \text{fm}^5, \quad \beta_{M2}^p = -24.33 \times 10^{-4} \, \text{fm}^5 \tag{128}$$

which can be compared to the $\mathcal{O}(q^3)$ heavy-baryon chiral predictions [33]

$$\alpha_{E2,\text{HB},q^3}^p = 22.1 \times 10^{-4} \, \text{fm}^5, \quad \beta_{M2,\text{HB},q^3}^p = -9.5 \times 10^{-4} \, \text{fm}^5. \tag{129}$$

In the case of the higher-order spin polarizabilities, the dispersion-theoretical treatment yields [33]

$$\gamma_{ET}^p = -0.15 \times 10^{-4} \, \text{fm}^6, \quad \gamma_{MT}^p = -0.09 \times 10^{-4} \, \text{fm}^6,$$
$$\gamma_{M3}^p = 0.09 \times 10^{-4} \, \text{fm}^6, \quad \gamma_{E3}^p = 0.06 \times 10^{-4} \, \text{fm}^6, \tag{130}$$

which can be compared to the $\mathcal{O}(q^3)$ heavy-baryon chiral predictions [33]

$$\gamma_{ET,\text{HB},q^3}^p = -0.37 \times 10^{-4} \, \text{fm}^6, \quad \gamma_{MT,\text{HB},q^3}^p = -0.03 \times 10^{-4} \, \text{fm}^6$$
$$\gamma_{M3,\text{HB},q^3}^p = 0.11 \times 10^{-4} \, \text{fm}^6, \quad \gamma_{E3,\text{HB},q^3}^p = 0.11 \times 10^{-4} \, \text{fm}^6. \tag{131}$$

We see then that the chiral predictions are generally in the right ballpark with the pattern of higher-order polarizabilities found via the dispersion-theoretical analysis, though certainly higher-order contributions are required to obtain real agreement.

# 5 Generalized Polarizabilities

As in all studies with electromagnetic probes, the possibilities to investigate the structure of the target are much greater if virtual photons are used, since the energy and three-momentum of the virtual photon can be varied independently. Moreover, the longitudinal component of the current operators entering the amplitude can be studied. The amplitude for virtual Compton scattering (VCS) off the proton, $T_{\mathrm{VCS}}^p$, is accessible in the reaction $e^-(k_i) + p(p_i) \to \gamma(q') + e^-(k_f) + p(p_f)$. In the one-photon-exchange approximation, the scattering amplitude consists of the Bethe-Heitler (BH) piece, where the real photon is emitted by the initial or final electrons, and the VCS contribution, $T = T_{\mathrm{BH}} + T_{\mathrm{VCS}}$ [144]. The use of a virtual photon in the initial state (four-momentum $q = k_i - k_f$) means that there are now twelve invariant functions required to describe $T_{\mathrm{VCS}}$ [145, 146, 147]. We shall work in the center-of-mass frame of the final-state photon-nucleon system, where we have

$$
\begin{aligned}
\mathbf{p}_f &= -\mathbf{q}', \\
\mathbf{p}_i &= -\mathbf{q} = -\bar{q}\,\hat{\mathbf{e}}_z, \\
\omega' + \sqrt{m_p^2 + \omega'^2} &= \omega + \sqrt{m_p^2 + \bar{q}^2},
\end{aligned}
\tag{132}
$$

with the $z$-axis defined by the three-momentum vector $\mathbf{q}$ of the incident virtual photon. Working in Lorenz gauge

$$
\epsilon \cdot q = 0, \quad \epsilon_0 = \frac{\bar{q}}{\omega}\epsilon_z
\tag{133}
$$

with $\boldsymbol{\epsilon} = \boldsymbol{\epsilon}_T + \epsilon_z \hat{\mathbf{e}}_z$, we can represent the VCS transition amplitude as

$$
\begin{aligned}
T_{\mathrm{VCS}} =\ & \hat{\boldsymbol{\epsilon}}'^* \cdot \boldsymbol{\epsilon}_T A_1 + \hat{\boldsymbol{\epsilon}}'^* \cdot \hat{\mathbf{q}}\, \boldsymbol{\epsilon}_T \cdot \hat{\mathbf{q}}' A_2 + i\boldsymbol{\sigma} \cdot (\hat{\boldsymbol{\epsilon}}'^* \times \boldsymbol{\epsilon}_T) A_3 + i\boldsymbol{\sigma} \cdot (\hat{\mathbf{q}}' \times \hat{\mathbf{q}})\, \hat{\boldsymbol{\epsilon}}'^* \cdot \boldsymbol{\epsilon}_T A_4 \\
& + i\boldsymbol{\sigma} \cdot (\hat{\boldsymbol{\epsilon}}'^* \times \hat{\mathbf{q}})\boldsymbol{\epsilon}_T \cdot \hat{\mathbf{q}}' A_5 + i\boldsymbol{\sigma} \cdot (\hat{\boldsymbol{\epsilon}}'^* \times \hat{\mathbf{q}}')\boldsymbol{\epsilon}_T \cdot \hat{\mathbf{q}}\, A_6 \\
& - i\boldsymbol{\sigma} \cdot (\boldsymbol{\epsilon}_T \times \hat{\mathbf{q}}')\hat{\boldsymbol{\epsilon}}'^* \cdot \hat{\mathbf{q}}\, A_7 - i\boldsymbol{\sigma} \cdot (\boldsymbol{\epsilon}_T \times \hat{\mathbf{q}})\hat{\boldsymbol{\epsilon}}'^* \cdot \hat{\mathbf{q}}\, A_8 \\
& + \frac{q^2}{\omega^2}\epsilon_z \left[ \hat{\boldsymbol{\epsilon}}'^* \cdot \hat{\mathbf{q}}\, A_9 + i\vec{\boldsymbol{\sigma}} \cdot (\hat{\mathbf{q}}' \times \hat{\mathbf{q}})\hat{\boldsymbol{\epsilon}}'^* \cdot \hat{\mathbf{q}}\, A_{10} \right. \\
& \left. + i\boldsymbol{\sigma} \cdot (\hat{\boldsymbol{\epsilon}}'^* \times \hat{\mathbf{q}})A_{11} + i\boldsymbol{\sigma} \cdot (\hat{\boldsymbol{\epsilon}}'^* \times \hat{\mathbf{q}}')A_{12} \right].
\end{aligned}
\tag{134}
$$

Here each amplitude $A_i$ ($i = 1, 2, \ldots, 12$) is a function of the three kinematic quantities $\omega', \bar{q}, \theta$.

Model-independent predictions, based on Lorentz invariance, gauge invariance, crossing symmetry, and the discrete symmetries, have been derived in Ref. [146]. Up to and including terms of second order in $\bar{q}$ and $\omega'$, the amplitude is completely specified in terms of quantities which can be obtained from other processes, namely $m_p$, $\kappa_p$, the electric and magnetic Sachs form factors $G_E^p$ and $G_M^p$, the electric mean square radius $\langle (r_E^p)^2 \rangle$, and the RCS polarizabilities $\alpha_E^p$ and $\beta_M^p$.

As in the case of real Compton scattering, each invariant amplitude can be written as the sum of "Born terms" and structure-dependent components

$$A_i(\omega', \bar{q}, \theta) = A_i^{\text{Born}}(\omega', \bar{q}, \theta) + A_i^{\text{structure}}(\omega', \bar{q}, \theta). \tag{135}$$

Here the Born term consists of the sum of the nucleon and anomaly ($\pi^0$ pole)

pieces [148, 149]—

$$A_1^{\text{Born}} = -\frac{e^2}{m_p} + \mathcal{O}(1/m_p^3),$$

$$A_2^{\text{Born}} = \bar{q}\frac{e^2}{m_p^2} + \mathcal{O}(1/m_p^3),$$

$$A_3^{\text{Born}} = \left[(1 + 2\kappa_p)\omega' - (1 + \kappa_p)^2\bar{q}\cos\theta\right]\frac{e^2}{2m_p^2}$$
$$- \frac{\omega'(\omega'^2 + \bar{q}^2 - 2\omega'\bar{q}\cos\theta)}{f(\omega', \bar{q}, \theta)}\frac{e^2 g_A}{8\pi^2 F_\pi^2} + \mathcal{O}(1/m_p^3),$$

$$A_4^{\text{Born}} = -(1 + \kappa_p)^2\bar{q}\frac{e^2}{2m_p^2} + \mathcal{O}(1/m_p^3),$$

$$A_5^{\text{Born}} = (1 + \kappa_p)^2\bar{q}\frac{e^2}{2m_p^2} - \frac{\omega'^2\bar{q}}{f(\omega', \bar{q}, \theta)}\frac{e^2 g_A}{8\pi^2 F_\pi^2} + \mathcal{O}(1/m_p^3),$$

$$A_6^{\text{Born}} = -(1 + \kappa_p)\omega'\frac{e^2}{2m_p^2} + \frac{\omega'^3}{f(\omega', \bar{q}, \theta)}\frac{e^2 g_A}{8\pi^2 F_\pi^2} + \mathcal{O}(1/m_p^3), \qquad (136)$$

$$A_7^{\text{Born}} = (1 + \kappa_p)^2\omega'\frac{e^2}{2m_p^2} - \frac{\omega'^2\bar{q}}{f(\omega', \bar{q}, \theta)}\frac{e^2 g_A}{8\pi^2 F_\pi^2} + \mathcal{O}(1/m_p^3),$$

$$A_8^{\text{Born}} = -(1 + \kappa_p)\frac{\bar{q}^2}{\omega'}\frac{e^2}{2m_p^2} + \frac{\omega'\bar{q}^2}{f(\omega', \bar{q}, \theta)}\frac{e^2 g_A}{8\pi^2 F_\pi^2} + \mathcal{O}(1/m_p^3),$$

$$A_9^{\text{Born}} = -\frac{e^2}{m_p} + \frac{2\omega'\bar{q}\cos\theta + \bar{q}^2}{\omega'}\frac{e^2}{2m_p^2} + \mathcal{O}(1/m_p^3),$$

$$A_{10}^{\text{Born}} = -\frac{\omega'^2\bar{q}}{f(\omega', \bar{q}, \theta)}\frac{e^2 g_A}{8\pi^2 F_\pi^2} + \mathcal{O}(1/m_p^3),$$

$$A_{11}^{\text{Born}} = (1 + 2\kappa_p)\omega'\frac{e^2}{2m_p^2} - \frac{\omega'^2(\omega' - \bar{q}\cos\theta)}{f(\omega', \bar{q}, \theta)}\frac{e^2 g_A}{8\pi^2 F_\pi^2} + \mathcal{O}(1/m_p^3),$$

$$A_{12}^{\text{Born}} = -(1 + \kappa_p)\cos\theta\,\omega'\frac{e^2}{2m_p^2} - \frac{\omega'^2(\bar{q} - \omega'\cos\theta)}{f(\omega', \bar{q}, \theta)}\frac{e^2 g_A}{8\pi^2 F_\pi^2} + \mathcal{O}(1/m_p^3),$$

where

$$f(\omega', \bar{q}, \theta) = M_\pi^2 + \omega'^2 + \bar{q}^2 - 2\omega'\bar{q}\cos\theta \qquad (137)$$

originates from the pion pole term.

After dividing the amplitude $T_{\text{VCS}}$ into a gauge-invariant generalized Born piece $T_{\text{VCS}}^{\text{Born}}$ and a structure-dependent residual component $T_{\text{VCS}}^{\text{R}}$, the so-called

*generalized* polarizabilities (GPs) of Ref. [145] result from an analysis of the residual term in terms of electromagnetic multipoles. A restriction to the lowest order, *i.e.*, terms linear in $\omega'$, leads to only electric and magnetic dipole radiation in the final state. Parity and angular-momentum selection rules, charge-conjugation symmetry, and particle crossing generate six independent GPs [145, 150, 151]. Predictions for the GPs of the nucleon have been obtained, for example, in the constituent quark model [145, 152], in HBChPT at $\mathcal{O}(q^3)$ [147, 153] and $\mathcal{O}(q^4)$ [154, 155], as well as in the small-scale expansion at $\mathcal{O}(q^3)$ [149]. The predictions of HBChPT at $\mathcal{O}(q^3)$ contain no unknown LECs, *i.e.*, they are given in terms of the pion mass, the axial-vector coupling constant $g_A$, and the pion-decay constant $F_\pi$. In the case of the spin-independent polarizabilities we have for the proton and the neutron

$$
\begin{aligned}
\alpha_E(\bar{q}^2) &= \frac{5e^2 g_A^2}{384\pi^2 F_\pi^2 M_\pi}\left(1 - \frac{7}{50}\frac{\bar{q}^2}{M_\pi^2} + \frac{81}{2800}\frac{\bar{q}^4}{M_\pi^4} + \dots\right), \\
\beta_M(\bar{q}^2) &= \frac{e^2 g_A^2}{768\pi^2 F_\pi^2 M_\pi}\left(1 + \frac{1}{5}\frac{\bar{q}^2}{M_\pi^2} - \frac{39}{560}\frac{\bar{q}^4}{M_\pi^4} + \dots\right).
\end{aligned}
\tag{138}
$$

Note that at $\bar{q} = 0$ the values of the generalized polarizabilities coincide with their real photon counterparts. In the case of the electric polarizability, the $\bar{q}^2$ dependence involves a general fall-off with the scale $\bar{q}^2/M_\pi^2$ as expected from the contribution of the pion cloud. After Fourier transforming we find that the local polarizability involves a maximum at the center and a falloff with size $\sim \delta \sim 1/M_\pi$. In the case of the magnetic polarizability, there is an *increase* in momentum space before a general falloff as expected from the pion-cloud contribution. Thus, there is a prediction of both paramagnetic and diamagnetic behavior.

A covariant definition of the spin-averaged dipole polarizabilities was proposed in Ref. [156]. It was shown that *three* generalized dipole polarizabilities are needed to reconstruct the location of the polarization by Fourier transforming. For example, if the nucleon is exposed to a static and uniform external electric field $\mathbf{E}$, an electric polarization $\mathcal{P}$ is generated which is related to the *density* of the induced electric dipole moments,

$$
\mathcal{P}_i(\mathbf{r}) = 4\pi\alpha_{ij}(\mathbf{r})\, E_j.
\tag{139}
$$

The tensor $\alpha_{ij}(\mathbf{r})$, *i.e.* the density of the full electric polarizability of the system, can be expressed as [156]

$$
\alpha_{ij}(\mathbf{r}) = \alpha_L(r)\frac{r_i r_j}{r^2} + \alpha_T(r)\frac{r^2\delta_{ij} - r_i r_j}{r^2} + \frac{3r_i r_j - r^2\delta_{ij}}{r^5}\int_r^\infty dr'r'^2[\alpha_L(r') - \alpha_T(r')],
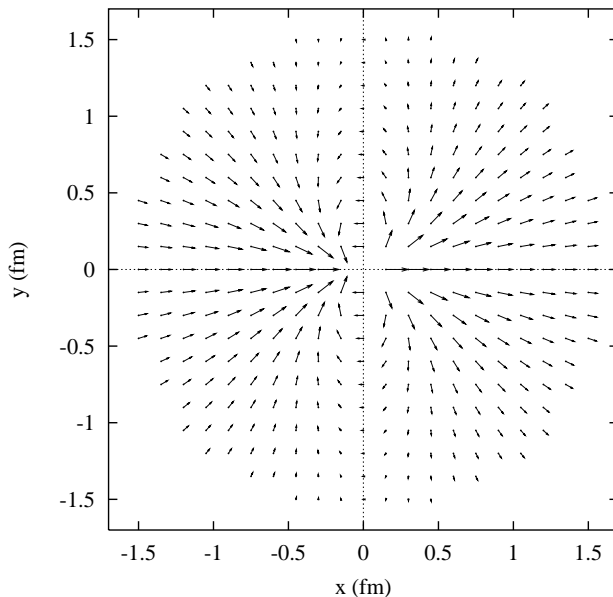$$

36

Figure 4: Scaled electric polarization $r^3\alpha_{i1}$ $[10^{-3}$ fm$^3]$ [157]. The applied electric field points in the $x$ direction.

where $\alpha_L(r)$ and $\alpha_T(r)$ are Fourier transforms of the generalized longitudinal and transverse electric polarizabilities $\alpha_L(q^2)$ and $\alpha_T(q^2)$, respectively. In particular, it is important to realize that both longitudinal and transverse polarizabilities are needed to fully recover the electric polarization $\mathcal{P}$. Figure 4 shows the induced polarization inside a proton as calculated in the framework of HBChPT at $\mathcal{O}(q^3)$ [157]. Since $\alpha_L(q^2)$ and $\alpha_T(q^2)$ differ, the polarization does not necessarily point into the direction of the applied electric field. Similar considerations apply to an external magnetic field. Since the magnetic induction is always transverse (*i.e.*, $\boldsymbol{\nabla} \cdot \mathbf{B} = 0$), it is sufficient to consider $\beta_{ij}(\mathbf{r}) = \beta(r)\delta_{ij}$ [156]. The induced magnetization $\mathcal{M}$ is given in terms of the density of the magnetic polarizability as $\mathcal{M}(\mathbf{r}) = 4\pi\beta(r)\mathbf{H}$.

On the experimental side, such experiments are extremely challenging since the cross section is dominated by the Bethe-Heitler and Born processes and the structure-dependent terms involving generalized polarizabilities represent small corrections. Expanding in terms of the final-state-photon center-of-mass energy, we have

$$d^5\sigma(pe\gamma) = d^5\sigma_{\text{BH+Born}} + \omega' \left[v_{LL}(P_{LL} - P_{TT}/\epsilon) + v_{LT}P_{LT}\right] + \mathcal{O}(\omega'^2), \quad (140)$$

37

where $d^5\sigma$ is shorthand for $d^5\sigma/dk'_{\text{lab}}d\Omega'_{e\,\text{lab}}d\Omega_{\gamma\text{cm}}$ and $v_{LL}$, $v_{LT}$ are known kinematic factors. The generalized polarizabilities are contained in the structure functions

$$
\begin{aligned}
P_{LL} - P_{TT}/\epsilon &= \frac{4m_p}{\alpha_{\text{em}}}G_E^p(Q^2)\alpha_E^p(Q^2) + \text{spin GPs,} \\
P_{LT} &= -\frac{2m_p}{\alpha_{\text{em}}}\sqrt{\frac{|\mathbf{q}_{cm}|^2}{Q^2}}G_E^p(Q^2)\beta_M^p(Q^2) + \text{spin GPs,}
\end{aligned}
\tag{141}
$$

where $G_E^p(Q^2)$ is the electric form factor of the proton. Despite the experimental challenges, the virtual Compton scattering process has been studied at MAMI [34, 37], at JLab [35, 39], and at Bates [36, 38], with results for the generalized polarizabilities $\alpha_E^p(Q^2)$, $\beta_M^p(Q^2)$ shown in Figure 5, where it can be seen that there exists rough agreement with the chiral expectations. However, experiments with increased statistics are clearly called for. Finally, the generalized polarizabilities of pions and kaons have been discussed in Refs. [156, 158, 159, 160].

# 6    Conclusion

Above we have studied various aspects of hadron polarizabilities, which measure the response of such systems to the imposition of electric and magnetizing fields, which are supplied in a Compton scattering process. In the case of the nucleon, the proton and neutron electric and magnetic (scalar) polarizabilities $\alpha_E$ and $\beta_M$, which arise at $\mathcal{O}(\omega^2)$ with respect to the leading Thomson amplitude, are found experimentally to be

$$
\alpha_E \simeq 6\beta_M \simeq 12 \times 10^{-4}\,\text{fm}^3
\tag{142}
$$

and are in line with what is expected from heavy-baryon chiral perturbative estimates, indicating the importance of the meson cloud in the nucleon analysis. In the case of the charged pion, chiral symmetry provides a strong constraint in terms of radiative pion beta decay and ChPT makes a firm prediction beyond the current-algebra result at the two-loop level. Both the experimental determination as well as the theoretical extraction from experiment require further efforts. We also have studied the higher-order manifestations of polarizabilities. At $\mathcal{O}(\omega^3)$ we have discussed the four spin polarizabilities, which are just now beginning to be measured at MAMI and
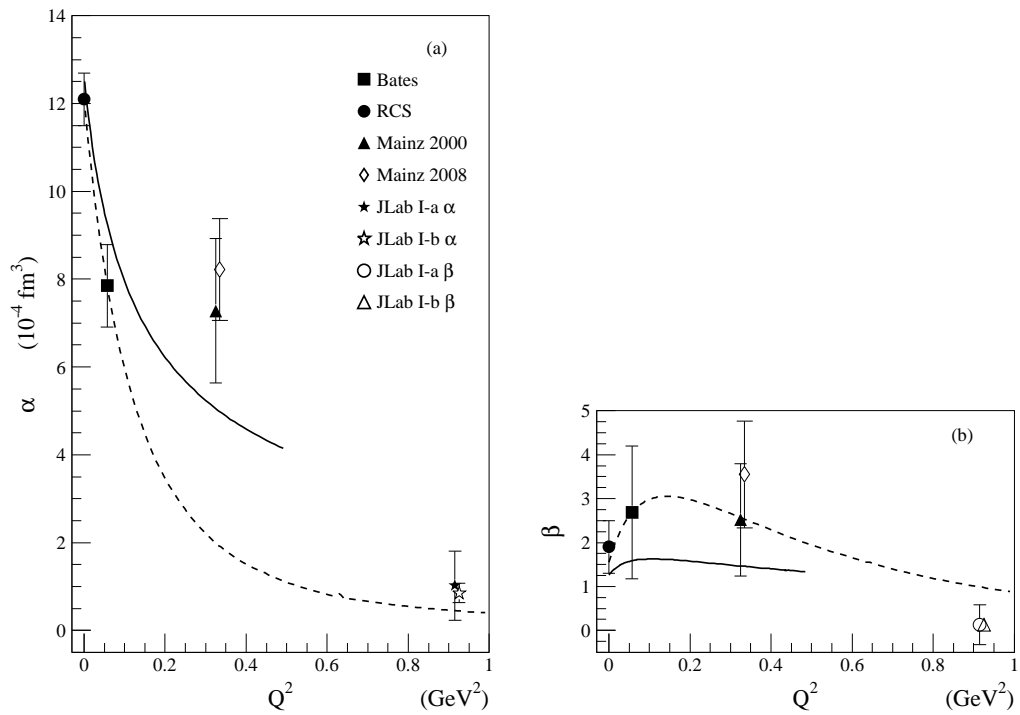
Figure 5: Left panel: Experimental data on $\alpha_E^p(Q^2)$. Right panel: Experimental data on $\beta_M^p(Q^2)$. The data are taken from Refs. [34, 35, 36, 37, 38, 39].

potentially at HIGS. We also looked at polarizabilities which arise at $\mathcal{O}(\omega^4)$ and higher and confronted chiral estimates with "measured" values from dispersion relations. Finally, we have looked at the generalized polarizabilities, which examine the local polarizability distributions. As a general observation we conclude that the gross picture is described by the lowest, nontrivial order in ChPT and precise measurements will provide valuable guidance for assessing the physics beyond lowest-order dynamics.

# Acknowledgment

# References

[1] Jackson JD. 1972. *Classical Electrodynamics*. New York: Wiley

[2] Klein A. 1955. Phys. Rev. 99: 998-1008

[3] Friar JL. 1988. Electromagnetic polarizabilities of hadrons. Proc. Workshop on Electron nucleus scattering, Marciana Marina, Italy, June 7-15, pp. 3-23. Singapore: World Scientific

[4] Holstein BR. 1990. Comments Nucl. Part. Phys. A 19: 221-238

[5] Holstein BR. 1992. Comments Nucl. Part. Phys. 20: 301-324

[6] L'vov AI. 1993. Int. J. Mod. Phys. A 8: 5267-5303

[7] Scherer S. 1999. Czech. J. Phys. 49: 1307-1345

[8] Drechsel D, Pasquini B, Vanderhaeghen M. 2003. Phys. Rept. 378: 99-205

[9] Schumacher M. 2005. Prog. Part. Nucl. Phys. 55: 567-646

[10] Downie EJ, Fonvieille H. 2011. Eur. Phys. J. ST 198: 287-306

[11] Federspiel, FJ, et al. 1991. Phys. Rev. Lett. 67: 1511-1514

[12] Zieger A, et al. 1992. Phys. Lett. B 278: 34-38

[13] MacGibbon BE, Garino G, Lucas MA, Nathan AM, Feldman G, Dolbilkin B. 1995. Phys. Rev. C 52: 2097-2109

[14] Blanpied G, et al. 2001. Phys. Rev. C 64: 025203

[15] Olmos de Leon V, et al. 2001. Eur. Phys. J. A 10: 207-215

[16] Schmiedmayer J, Riehs P, Harvey JA, Hill NW. 1991. Phys. Rev. Lett. 66: 1015-1018

[17] Rose KW, et al. 1990. Nucl. Phys. A 514: 621-648

[18] Kossert K, et al. 2003. Eur. Phys. J. A 16: 259-273

[19] Lundin M, et al. 2003. Phys. Rev. Lett. 90: 192501

[20] Antipov YM, et al. 1983. Phys. Lett. B 121: 445-448

[21] Antipov YM, et al. 1985. Z. Phys. C 26: 495-497

[22] Aibergenov TA, et al. 1986. Czech. J. Phys. B 36: 948-851

[23] Babusci D, et al. 1992. Phys. Lett. B 277: 158-162

[24] Ahrens J, et al. 2005. Eur. Phys. J. A 23: 113-127

[25] Friedrich J. 2013. PoS Bormio 2013: 030

[26] Beringer J, et al. [Particle Data Group]. 2012. Phys. Rev. D 86: 010001 and 2013 partial update for the 2014 edition

[27] Nevado D, Pineda A. 2008. Phys. Rev. C 77: 035202

[28] Birse MC, McGovern JA. 2012. Eur. Phys. J. A 48: 120

[29] Engel KT, Patel HH, Ramsey-Musolf MJ. 2012. Phys. Rev. D 86: 037502

[30] Ragusa S. 1993. Phys. Rev. D 47: 3757-3767

[31] Ragusa S. 1994. Phys. Rev. D 49: 3157-3159

[32] Babusci D, Giordano G, L'vov AI, Matone G, Nathan AM. 1998. Phys. Rev. C 58: 1013-1041

[33] Holstein BR, Drechsel D, Pasquini B, Vanderhaeghen M. 2000. Phys. Rev. C 61: 034316

[34] Roche J, et al. [VCS and A1 Collaborations]. 2000. Phys. Rev. Lett. 85: 708-711

[35] Laveissiere G, et al. [Jefferson Lab Hall A Collaboration]. 2004. Phys. Rev. Lett. 93: 122001

[36] Bourgeois P, et al. 2006. Phys. Rev. Lett. 97: 212001

[37] Janssens P, et al. [A1 Collaboration]. 2008. Eur. Phys. J. A 37: 1-8

[38] Bourgeois P, et al. 2011. Phys. Rev. C 84: 035206

[39] Fonvieille H, et al. [Jefferson Lab Hall A Collaboration]. 2012. Phys. Rev. C 86: 015210

[40] L'vov AI, Petrun'kin VA, Schumacher M. 1997. Phys. Rev. C 55: 359-377

[41] Drechsel D, Gorchtein M, Pasquini B, Vanderhaeghen M. 1999. Phys. Rev. C 61: 015204

[42] Gasser J, Leutwyler H. 1984. Annals Phys. 158: 142-210

[43] Gasser J, Sainio ME, Švarc A. 1988. Nucl. Phys. B 307: 779-853

[44] Brandt S, Dahmen HD. 2005. *Elektrodynamik*. Berlin: Springer. 4th ed.

[45] Merzbacher E. 1972. *Quantum Mechanics*. New York: Wiley

[46] Feynman RP, Leighton R, Sands M. 1964. *The Feynman Lectures on Physics*, Vol. 2, Sec. 34-4. Reading, MA: Addison-Wesley

[47] Holstein BR. 1992. *Topics in Advanced Quantum Mechanics*. Reading, MA: Addison-Wesley

[48] Powell JL. 1949. Phys. Rev. 75: 32-34

[49] Beane SR, Malheiro M, McGovern JA, Phillips DR, van Kolck U. 2003. Phys. Lett. B 567: 200-206

[50] Lensky V, Pascalutsa V. 2010. Eur. Phys. J. C 65: 195-209

[51] McGovern JA, Phillips DR, Grießhammer HW. 2013. Eur. Phys. J. A 49: 12

[52] Mukhopadhyay NC, Nathan AM, Zhang L. 1993. Phys. Rev. D 47: 7-10

[53] Scherer S, Mulders PJ. 1992. Nucl. Phys. A 549: 521-536

[54] Gell-Mann M, Goldberger ML, Thirring WE. 1954. Phys. Rev. 95: 1612-1627

[55] Titchmarsh EC. 1962. *Introduction to the theory of Fourier integrals.* Oxford: Clarendon Press, 2nd ed.

[56] Baldin AM. 1960. Nucl. Phys. 18: 310-317

[57] Babusci D, Giordano G, Matone G. 1998. Phys. Rev. C 57: 291-294

[58] Levchuk MI, L'vov AI. 2000. Nucl. Phys. A 674: 449-492

[59] Bernabeu J, Ericson TEO, Ferro Fontan C. 1974. Phys. Lett. B 49: 381-384

[60] Bernabeu J, Tarrach R. 1977. Phys. Lett. B 69: 484-488

[61] Schumacher M, Scadron MD. 2013. Fortsch. Phys. 61: 703-741

[62] Holstein BR, Nathan AM. 1994. Phys. Rev. D 49: 6101-6108

[63] Baru V, Hanhart C, Hoferichter M, Kubis B, Nogga A, Phillips DR. 2011. Phys. Lett. B 694: 473-477

[64] Schumacher M. 2011. J. Phys. G 38: 083001

[65] Drechsel D, Russo A. 1984. Phys. Lett. B 137: 294-298

[66] Petrunkin VA. 1964. Nucl. Phys. 55: 197-206

[67] Ericson TEO, Hüfner J. 1973. Nucl. Phys. B 57: 604-616

[68] Friar JL. 1975. Annals Phys. 95: 170-201

[69] Weinberg S. 1979. Physica A 96: 327-340

[70] Ecker G. 1995. Prog. Part. Nucl. Phys. 35: 1-80

[71] Bernard V, Kaiser N, Meißner UG. 1995. Int. J. Mod. Phys. E 4: 193-346

[72] Scherer S. 2003. Adv. Nucl. Phys. 27: 277-546

[73] Scherer S, Schindler MR. 2012. Lect. Notes Phys. 830: 1-338

[74] Manohar A, Georgi H. 1984. Nucl. Phys. B 234: 189-212

[75] Donoghue JF, Golowich E, Holstein BR. 1984. Phys. Rev. D 30: 587-593

[76] Bernard V, Kaiser N, Meißner UG. 1991. Phys. Rev. Lett. 67: 1515-1518

[77] Jenkins EE, Manohar AV. 1991. Phys. Lett. B 255: 558-562

[78] Bernard V, Kaiser N, Kambor J, Meißner UG. 1992. Nucl. Phys. B 388: 315-345

[79] Bernard V, Kaiser N, Schmidt A, Meißner UG. 1993. Phys. Lett. B 319: 269-275

[80] Bernard V, Kaiser N, Meißner UG, Schmidt A. 1994. Z. Phys. A 348: 317-325

[81] Hemmert TR, Holstein BR, Kambor J. 1997. Phys. Rev. D 55: 5598-5612

[82] Pascalutsa V, Phillips DR. 2003. Phys. Rev. C 67: 055202

[83] Becher T, Leutwyler H. 1999. Eur. Phys. J. C 9: 643-671

[84] Schindler MR, Gegelia J, Scherer S. 2004. Phys. Lett. B 586: 258-266

[85] Gegelia J, Japaridze G. 1999. Phys. Rev. D 60: 114038

[86] Fuchs T, Gegelia G, Japaridze G, Scherer S. 2003. Phys. Rev. D 68: 056005

[87] Metz A, Drechsel D. 1996. Z. Phys. A 356: 351-357

[88] Kroll NM, Ruderman MA. 1954. Phys. Rev. 93: 233-238

[89] Krupina N, Pascalutsa V. 2013. Phys. Rev. Lett. 110: 262001

[90] Phillips DR. 2009. J. Phys. G 36: 104004

[91] Bernard V, Kaiser N, Kambor J, Meißner UG. 1992. Phys. Rev. D 46: 2756-2758

[92] Gasser J, Leutwyler H. 1985. Nucl. Phys. B 250: 465-516

[93] Volkov MK, Pervushin VN. 1975. Sov. J. Nucl. Phys. 22: 179-183

[94] Bijnens J, Cornet F. 1988. Nucl. Phys. B 296: 557-568

[95] Terent'ev MV. 1973. Sov. J. Nucl. Phys. 16: 87-93

[96] Donoghue JF, Holstein BR. 1989. Phys. Rev. D 40: 2378-2388

[97] Donoghue JF, Holstein BR. 1993. Phys. Rev. D 48: 137-146

[98] Wess J, Zumino B. 1971. Phys. Lett. B 37: 95-97

[99] Witten E. 1983. Nucl. Phys. B 223: 422-432

[100] Bijnens J. 1993. Int. J. Mod. Phys. A 8: 3045-3105

[101] Bychkov M, et al. 2009. Phys. Rev. Lett. 103: 051802

[102] Petrun'kin VA. 1981. Sov. J. Part. Nucl. 12: 278

[103] Bürgi U. 1996. Phys. Lett. B 377: 147-152

[104] Bürgi U. 1996. Nucl. Phys. B 479: 392-426

[105] Gasser J, Ivanov MA, Sainio ME. 2006. Nucl. Phys. B 745: 84-108

[106] Miskimen R. Private communication

[107] Marsiske H, et al. [Crystal Ball Collaboration]. 1990. Phys. Rev. D 41: 3324-3335

[108] Uehara S, et al. [Belle Collaboration]. 2008. Phys. Rev. D 78: 052004

[109] Donoghue JF, Holstein BR, Lin YC. 1988. Phys. Rev. D 37: 2423-2430

[110] Bellucci S, Gasser J, Sainio ME. 1994. Nucl. Phys. B 423: 80-122

[111] Bel'kov AA, Lanyov AV, Scherer S. 1996. J. Phys. G 22: 1383-1394

[112] Gasser J, Ivanov MA, Sainio ME. 2005. Nucl. Phys. B 728: 31-54

[113] Fil'kov LV, Kashevarov VL. 2005. Phys. Rev. C 72: 035211

[114] Pasquini B, Drechsel D, Scherer S. 2008. Phys. Rev. C 77: 065211

[115] Garcia-Martin R, Moussallam B. 2010. Eur. Phys. J. C 70: 155

[116] Hoferichter M, Phillips DR, Schat C. 2011. Eur. Phys. J. C 71: 1743

[117] Donoghue JF, Holstein BR. 1989. Phys. Rev. D 40: 3700-3707

[118] Guerrero F, Prades J. 1997. Phys. Lett. B 405: 341-346

[119] Backenstoss G, et al. 1973. Phys. Lett. B 43: 431-436

[120] Moinester M [COMPASS Collaboration]. 2003. Czech. J. Phys. 53: B169-B187

[121] Gell-Mann M, Goldberger ML. 1954. Phys. Rev. 96: 1433-1438

[122] Low FE. 1954. Phys. Rev. 96: 1428-1432

[123] Hemmert TR, Holstein BR, Kambor J, Knöchlein G. 1998. Phys. Rev. D 57: 5746-5754

[124] Gellas GC, Hemmert TR, Meißner UG. 2000. Phys. Rev. Lett. 85: 14-17

[125] Vijaya Kumar KB, McGovern JA, Birse MC. 2000. Phys. Lett. B 479: 167-172

[126] Kondratyuk S, Scholten O. 2001. Phys. Rev. C 64: 024005

[127] Gasparyan AM, Lutz MFM, Pasquini B. 2011. Nucl. Phys. A 866: 79-92

[128] Gerasimov SB. 1966. Sov. J. Nucl. Phys. 2: 430-433

[129] Drell SD, Hearn AC. 1966. Phys. Rev. Lett. 16: 908-911

[130] Ahrens J, et al. 2000. Phys. Rev. Lett. 84: 5950-5954

[131] Ahrens J, et al. 2001. Phys. Rev. Lett. 87: 022003

[132] Dutz H, et al. 2003. Phys. Rev. Lett. 91: 192001

[133] Dutz H, et al. 2004. Phys. Rev. Lett. 93: 032003

[134] Drechsel D, Walcher T. 2008. Rev. Mod. Phys. 80: 731-785

[135] Drechsel D, Hanstein O, Kamalov SS, Tiator L. 1999. Nucl. Phys. A 645: 145-174

[136] Arndt RA, Briscoe WJ, Strakovsky II, Workman RL. 2002. Phys. Rev. C 66: 055213

[137] Bianchi N, Thomas E. 1999. Phys. Lett. B 450: 439-447

[138] Simula S, Osipenko M, Ricco G, Taiuti M. 2002. Phys. Rev. D 65: 034017

[139] Arends HJ. Private communication

[140] Middleton D, Martel PP. 2013. PoS Bormio 2013: 039

[141] Grießhammer HW, Hemmert TR. 2002. Phys. Rev. C 65: 045207

[142] Hildebrandt RP, Grießhammer HW, Hemmert TR, Pasquini B. 2004. Eur. Phys. J. A 20: 293-315

[143] Pasquini B, Pedroni P, Drechsel D. 2010. Phys. Lett. B 687: 160-166

[144] Berg RA, Lindner CN. 1961. Nucl. Phys. 26: 259-279

[145] Guichon PAM, Liu GQ, Thomas AW. 1995. Nucl. Phys. A 591: 606-638

[146] Scherer S, Korchin AY, Koch JH. 1996. Phys. Rev. C 54: 904-919

[147] Hemmert TR, Holstein BR, Knöchlein G, Scherer S. 1997. Phys. Rev. D 55: 2630-2643

[148] Knöchlein G. *Virtual Compton Scattering off the Nucleon and Chiral Perturbation Theory.* Aachen: Shaker

[149] Hemmert TR, Holstein BR, Knöchlein G, Drechsel D. 2000. Phys. Rev. D 62: 014013

[150] Drechsel D, Knöchlein G, Metz A, Scherer S. 1997. Phys. Rev. C 55: 424-430

[151] Drechsel D, Knöchlein G, Korchin AY, Metz A, Scherer S. 1998. Phys. Rev. C 57: 941-952

[152] Pasquini B, Scherer S, Drechsel D. 2001. Phys. Rev. C 63: 025205

[153] Hemmert TR, Holstein BR, Knöchlein G, Scherer S. 1997. Phys. Rev. Lett. 79: 22-25

[154] Kao CW, Vanderhaeghen M. 2002. Phys. Rev. Lett. 89: 272002

[155] Kao CW, Pasquini B, Vanderhaeghen M. 2004. Phys. Rev. D 70: 114004

[156] L'vov AI, Scherer S, Pasquini B, Unkmeir C, Drechsel D. 2001. Phys. Rev. C 64: 015203

[157] L'vov AI, Scherer S. unpublished

[158] Unkmeir C, Scherer S, L'vov AI, Drechsel D. 2000. Phys. Rev. D 61: 034002

[159] Fuchs T, Pasquini B, Unkmeir C, Scherer S. 2002. Czech. J. Phys. 52: B135-B144

[160] Unkmeir C, Ocherashvili A, Fuchs T, Moinester MA, Scherer S. 2002. Phys. Rev. C 65: 015206